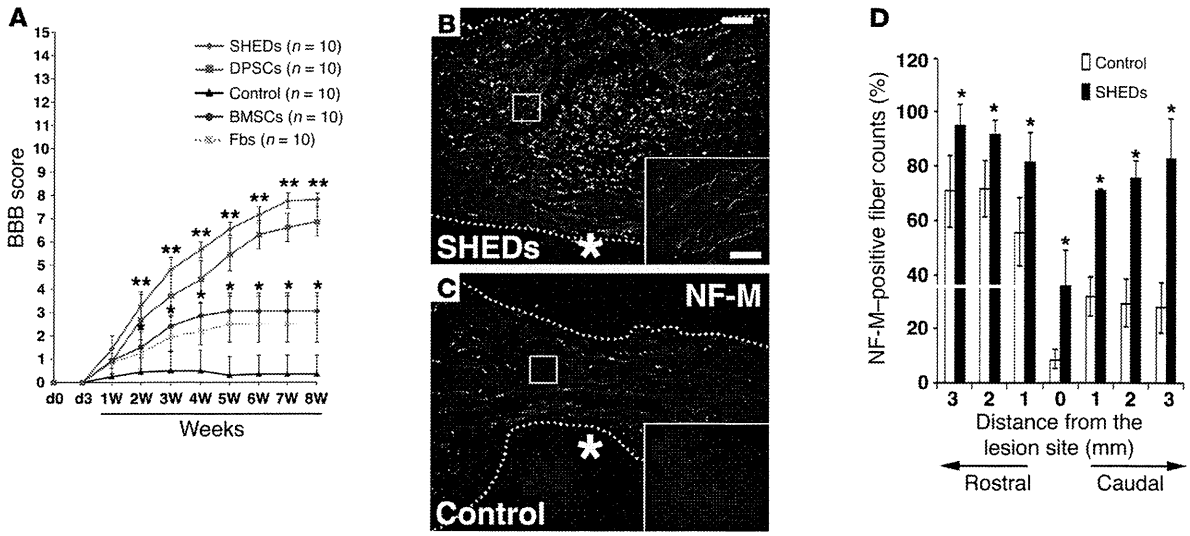

Figure 2

Engrafted SHEDs promote functional recovery of the completely transected SC. (**A**) Time course of functional recovery of hind limbs after complete transection of the SC. A total of 1 × 10^6 SHEDs, DPSCs, BMSCs, or fibroblasts were transplanted into the SCI immediately after transection. Data represent the mean ± SEM. $^{**}P < 0.001$, $^{*}P < 0.01$ compared with SCI models injected with PBS. (**B–D**) Representative images (**B** and **C**) and quantification (**D**) of NF-M–positive nerve fibers in sagittal sections of a completely transected SC, at 8 weeks after SCI. Dashed lines outline the SC. Insets are magnified images of boxed areas in **B** and **C**. (**D**) Nerve fiber quantification, representing the average of 3 experiments performed under the same conditions. The *x* axis indicates specific locations along the rostrocaudal axis of the SC (3 mm rostral and caudal to the epicenter), and *y* axis indicates the percentage of NF-M–positive fibers compared with that of the sham-operated SCs at the ninth thoracic spinal vertebrate (Th9) level. Data represent the mean ± SEM. $^{*}P < 0.05$ compared with SCI models injected with PBS. Scale bars: 100 μm and inset 20 μm (**B**) and 50 μm (**C**). Asterisks in **B** and **C** indicate the epicenter of the lesion.

by paracrine mechanisms; and (c) replacement of lost or damaged oligodendrocytes after SCI through specific differentiation into mature oligodendrocytes under the extreme conditions of SCI. To our knowledge, the latter two neuroregenerative activities (b and c) are unique to tooth-derived stem cells and are not exhibited by any other previously described stem cells. Thus, our data demonstrate that tooth-derived stem cells may provide significant therapeutic benefits for treating the acute phase of SCI through both cell-autonomous and paracrine/trophic regenerative activities.

Adult MSCs have been isolated from various tissues, including bone marrow, adipose tissue, skin, umbilical cord, and placenta (27–30). The therapeutic benefits of these stem cells have drawn intense attention in the field of translational medicine. Nevertheless, their biological equivalency/heterogeneity and identity are largely unknown (31). Tooth-derived stem cells exhibited BMSC-like multipotency and cell surface marker expression; however, they expressed a distinct set of multiple early neural linage markers (Table 1 and Figure 1). A cDNA microarray gene expression analysis showed that the SHEDs expressed many genes in the categories of extracellular and cell surface region, cell proliferation, and tissue/embryonic development, at levels at least 2-fold higher than BMSCs (Table 2). These data indicate that tooth-derived stem cells belong to a highly proliferative ectomesenchymal stem cell–like population that actively communicates with neighboring cells. These characteristics raise the question of what the role of these stem cells is in tooth development and maintenance. Although we do not have a clear answer at present, future analyses using model animals such as dogs and pigs may clarify their precise origin and normal functions, as well as identifying the physiological system that maintains the "stemness" of these cells in vivo.

Both axon regeneration and the reformation of appropriate neuronal connections are prerequisites for functional recovery from SCI. However, multiple AGIs block the inherent regenerative activities of injured axons (2–4). It is well known that multiple AGIs constitute a remarkably intricate molecular network in the extracellular space of the injured CNS, in which they activate a common intracellular signaling mediator, Rho GTPase, and its effector, Rho-associated kinase (ROCK) (32–36). The activation of the Rho-ROCK cascade induces growth cone collapse and axonal repulsion (37). The inactivation of Rho by C3 transferase or of ROCK by Y-27632 downregulates AGI signaling and promotes functional recovery after SCI (38–40). Thus, Rho/ROCK signaling is an important target for SCI treatments; however, no reports have yet described an effect of stem cell transplantation on regulating the multiple AGIs/Rho/ROCK signaling cascades. We found that engrafted SHEDs promoted the regeneration of two major types of descending axons (CST and 5-HT) beyond the lesion epicenter and concomitantly inhibited the SCI-induced Rho activation (Figure 4). Furthermore, both SHED-CM and DPSC-CM promoted the neurite extension of CGNs cultured on two different AGIs, CSPG and MAG (Figure 5). Taken together, these results strongly suggest that tooth-derived stem cells promote the regeneration of transected axons through the direct inhibition of multiple AGI signals by paracrine mechanisms. Notably, in contrast to the CMs from tooth-derived stem cells, BMSC-CM showed only a subtle anti-AGI activity in the neurite extension assay, in good agreement with the level of functional recovery observed in BMSC-transplanted rats. Thus, the anti-AGI activity of tooth-derived stem cells is one of their major therapeutic benefits for the treatment of SCI.

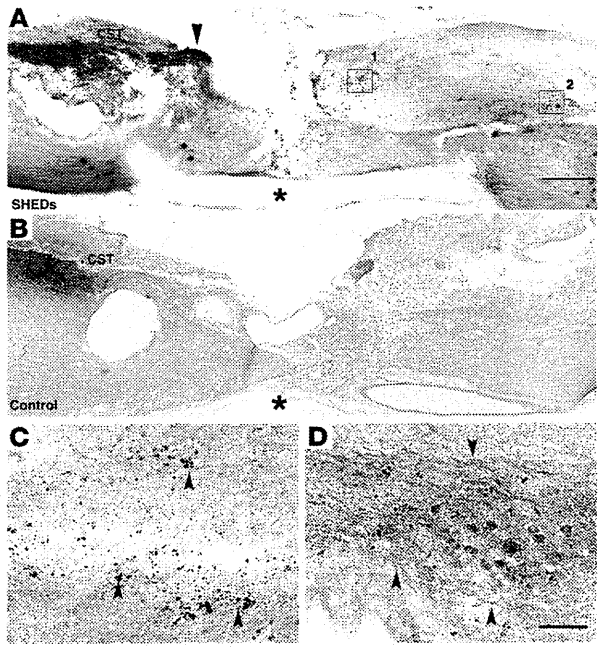

Figure 3
SHEDs regenerate CST fibers. Representative images of BDA-labeled CST axons. BDA-positive axons extended beyond the epicenter in the SHED-transplanted (**A**), but not the control SC (**B**). **C** and **D** are high-magnification views of boxed areas 1 and 2 in **A**, respectively. BDA-positive boutons were detected on the neurons of the caudal stump. Scale bars: 500 (**A**) and 100 μm (**D**). Arrowhead in **A** indicates abundant penetration of CST axons into the scar tissue of the rostral stump. Arrowheads in **C** and **D** indicate regenerated CST axons extended beyond the epicenter. Asterisks in **A** and **B** indicate the epicenter of the lesion.

The mechanisms that underlie the inhibition of multiple AGIs by SHED-CM and DPSC-CM are currently unknown. Although both SHEDs and DPSCs expressed an array of neurotrophic factors (Figure 1), our preliminary analysis showed that these trophic factors alone failed to promote the neurite extension of CGNs cultured on CSPG-coated dishes (K. Sakai and A. Yamamoto, unpublished observations). These results suggest that unknown factors, rather than neurotrophic factors, expressed by SHEDs and/or DPSCs may play major roles in the inhibition of multiple AGI signaling pathways. Since the strong anti-AGI activity was unique to the tooth-derived stem cells, but not to BMSCs, extracellular-related genes being preferentially expressed in SHEDs relative to BMSCs (Table 2) is a possible candidate anti-AGI factor. Future functional analysis of these genes will be required to reveal the molecular mechanisms by which tooth-derived stem cells regulate multiple AGI activities to promote the regeneration of injured axons.

It has been shown that pharmacological blockade of neuron and/or oligodendrocyte apoptosis by erythropoietin (41, 42), inhibitors of purine receptor P2X7 (OxATP and PPADS) (43), a neutralizing Ab against CD95 (FAS) antigen (44), or minocycline (45, 46) promotes functional recovery after SCI. We found that engrafted SHEDs suppressed the apoptosis of both neurons and oligodendrocytes (Figure 8), which resulted in the remarkable preservation of neurofilaments and myelin sheaths in the region surrounding the epicenter (Figures 2 and 6). Notably, in addition to these two cell lineages, SHEDs strongly inhibited the apoptosis of astrocytes recruited to the lesion. In the classical view, reactive, CSPG-generating astrocytes are considered to be an obstacle to axon regeneration; however, recent genetic studies in mice have shown that the conditional ablation of astrocytes after SCI resulted in larger lesions, failure of blood brain barrier repair, expansion of the inflammatory response and tissue disruption, severe demyelination, and profound cell death of neurons and oligodendrocytes (47–51). Thus, the accumulated evidence demonstrates that, in addition to their anti-regenerative activity, astrocytes play an important role in the neuroprotection during the acute phase of SCI. We found that SHEDs suppressed the apoptosis of astrocytes and minimized secondary injury but inhibited AGI activity of CSPG derived from activated astrocytes. Thus, these results demonstrate that SHEDs promote the neuroprotective role but inhibit the anti-neuroregenerative activity of astrocytes to promote functional recovery after SCI.

Figure 4
SHEDs regenerate 5-HT fibers and inhibit SCI-induced activation of Rho GTPase. (**A–D**) Representative images (**A–C**) and quantification (**D**) of serotonergic raphe axons stained with 5-HT mAb in the sagittal sections of the transected SC. A large number of 5-HT axons penetrated the scar tissue of the rostral stump in the SHED-transplanted SC (**A**), while only a few did in the control transected SC (**B**). (**C**) 5-HT–positive boutons were in contact with neurons of the caudal stump. Arrowhead indicates 5-HT–positive fiber extended beyond the epicenter. Quantification of regenerated 5-HT axons (**D**) was carried out as described in Figure 2D, except the *y* axis indicates the percentage of 5-HT axons compared with that in the sham-operated SC. Data represent the mean ± SEM. $^*P < 0.01$ compared with SCI models injected with PBS. Scale bars: 50 μm (**B** and **C**). (**E**) SCI-induced Rho GTPase activation 7 days after SCI was suppressed by engrafted SHEDs. The level of active Rho in lysate from the samples indicated at the top (sham-operated, control, and SHED-transplanted) was examined by RBD pull-down assay.

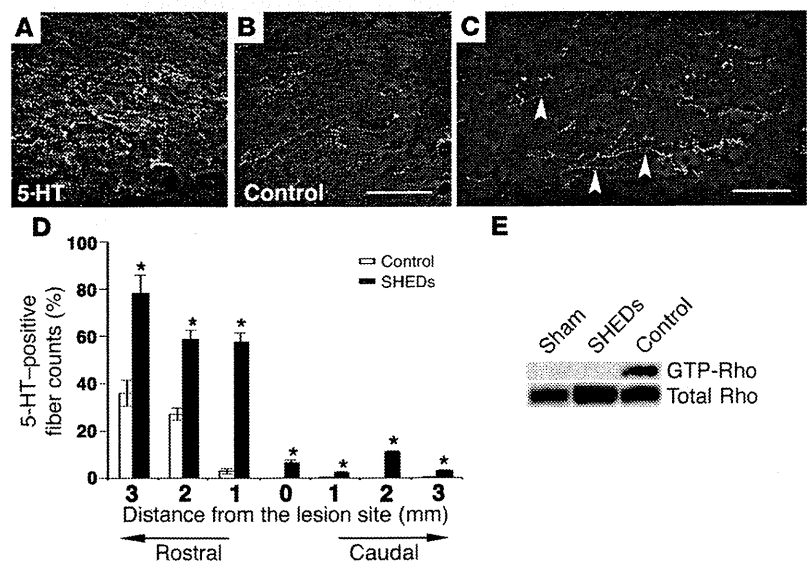

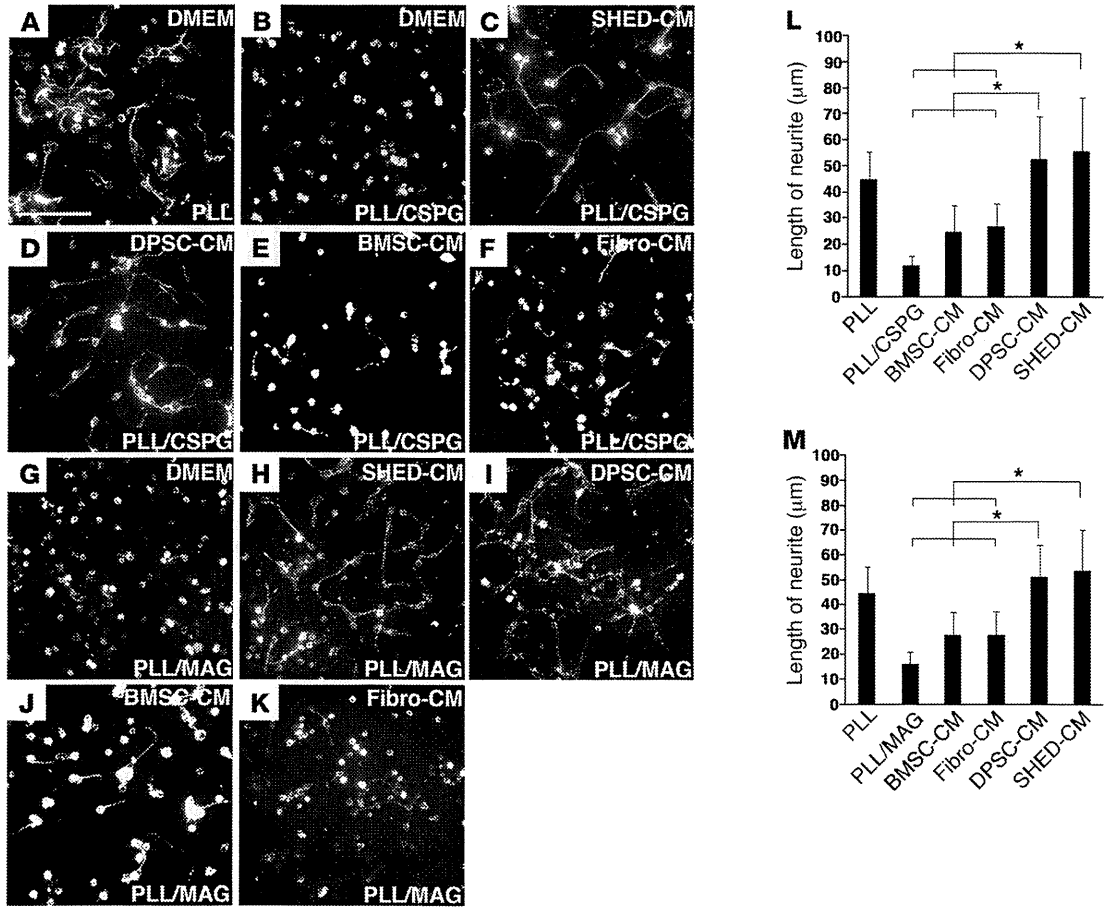

Figure 5

SHED-CM and DPSC-CM promote the neurite extension of CGNs on CSPG or MAG. CGNs were plated on PLL (**A**), PLL /CSPG (**B**–**F**), or PLL /MAG (**G**–**K**), with the CM indicated at the top of each panel. CGNs plated with SHED-CM or DPSC-CM extended their neurites on the CSPG- (**C** and **D**) and MAG-coated (**H** and **I**) dishes, while BMSC-CM and fibroblast-CM (Fibro-CM) elicited only marginal extension on CSPG (**E** and **F**) and MAG (**J** and **K**). Quantification of the neurite length of CGNs plated on CSPG (**L**) and MAG (**M**). The *y* axis indicates the neurite length. Data represent the average measurements for each cell type from 3 independent donors. This set of experiments was performed 3 times and yielded similar results. Error bars represent SD. $^*P < 0.05$. Scale bar in **A** is 100 μm.

Our data revealed two major advantages of using SHEDs for cell replacement in SCI treatment. First, we observed good survival of the engrafted SHEDs: more than 30% of the engrafted SHEDs survived as a cell mass in the injured SC. A previous study reported that, although the experimental details differed from ours, the survival rate of human ES cell–derived oligodendrocytes or motor neurons, transplanted just after complete SC transection, is less than 1% (8). We speculate that the SHED-mediated minimization of secondary injury and/or the formation of cohesive cell clusters of engrafted SHEDs may be attributable to their excellent cell survival rate. Second, we observed that the engrafted SHEDs specifically differentiated toward mature oligodendrocytes, expressing APC and MBP. It has been shown that DPSCs and SHEDs differentiate in vitro toward functionally active neurons that express voltage-gated Na^+ channels and in vivo toward neuron-like cells 48 hours after their transplantation into the mesencephalon of avian embryos (18). Taken together with our findings, these results support the idea that tooth-derived stem cells exhibit neural stem cell–like characteristics and that unknown environmental cues are important for their fate determination. Since cell-based remyelination strategies can restore saltatory conduction and promote functional recovery after SCI (52), the SHED's strong cell survival and oligodendrocyte-specific differentiation potential, particularly under the extreme conditions of SCI, would be great advantages in using these cells to treat SCI. It is hoped that in the future, clarification of the regulatory cues for the specific differentiation of SHEDs will help us to establish efficient therapeutic protocols for SCI patients based on precise cell fate control.

The aim of this study was to address the neuroregenerative activity of tooth-derived stem cells in a particular CNS injury model, SCI. We used the rat complete transection model, because it provides good reproducibility and permits a more accurate assessment of the effects of treatment than do other SCI models. Although contusion and crush models would provide experimental conditions that are closer to the SCIs seen clinically in humans, the amount of injury in these models is not consistent from animal to animal. Furthermore, these incomplete transection models permit spontaneous recovery after SCI, and the residual SC tissues may provide routes for the compensatory sprouting of uninjured SC axons (53). Thus, the transection model was cho-

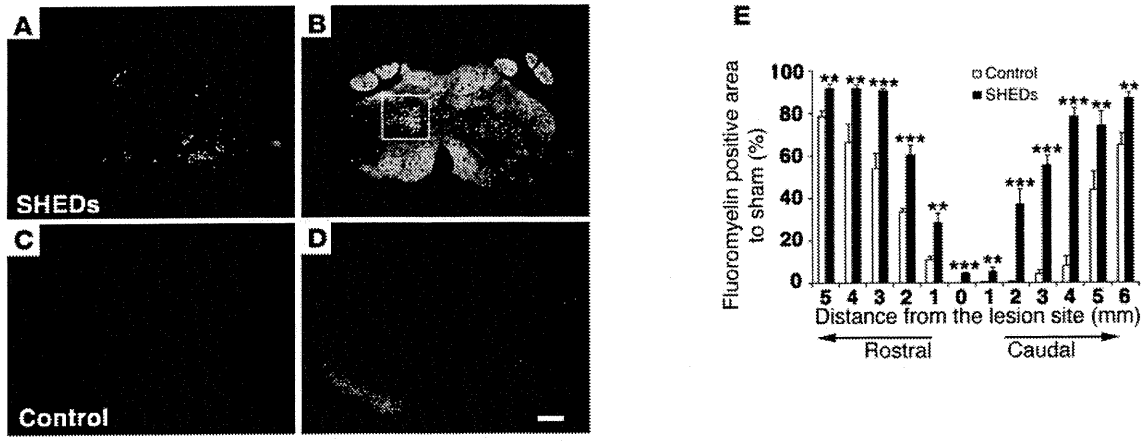

Figure 6
SHEDs preserve myelin sheath and differentiate into mature oligodendrocytes in the transected SC. Representative images (**A**–**D**) and quantification (**E**) of the myelinated area 8 weeks after SCI. Transverse sections of the epicenter (**A** and **C**) and 3 mm caudal to it (**B** and **D**) were stained with FluoroMyelin. The myelinated area in both regions was significantly preserved in the SHED-transplanted SC (**A** and **B**), but abolished in the control SC (**C** and **D**). Scale bar: 100 μm (**D**). (**E**) Quantification of the myelinated area showing the average of 3 experiments performed in parallel. The *x* axis indicates specific locations along the rostrocaudal axis of the SC. The *y* axis indicates the percentage of the myelin-positive area compared with that of the sham-operated SC at the Th9 level. Error bars represent SD. $^{*}P < 0.05$, $^{**}P < 0.01$, $^{***}P < 0.001$ compared with SCI models injected with PBS.

sen as most appropriate for the precise assessment of the axonal regeneration activity of tooth-derived stem cells.

In this study, we transplanted cells into the injured SC immediately after surgical transection, which is impractical for most human SCI cases. We chose this system to examine the therapeutic benefits of the transplanted cells in countering the multiple pathogenic signals that function synergistically during the early phase of SCI. Our future studies will analyze the neuroregenerative activities of tooth-derived stem cells in SCI under more clinically relevant experimental conditions.

In conclusion, we demonstrated multifaceted neuroregenerative activities of tooth-derived stem cells that fulfill many requirements for functional recovery after SCI. Not only did engrafted SHEDs have remarkable neuroregenerative activities, they also showed no malignant transformation 8 weeks after implantation (data not shown). Furthermore, SHEDs and DPSCs can be obtained from exfoliated deciduous and impacted adult wisdom teeth without adverse health effects. Thus, there are few ethical concerns regarding their clinical use. We propose that tooth-derived stem cells may be an excellent and practical cellular resource for the treatment of SCI.

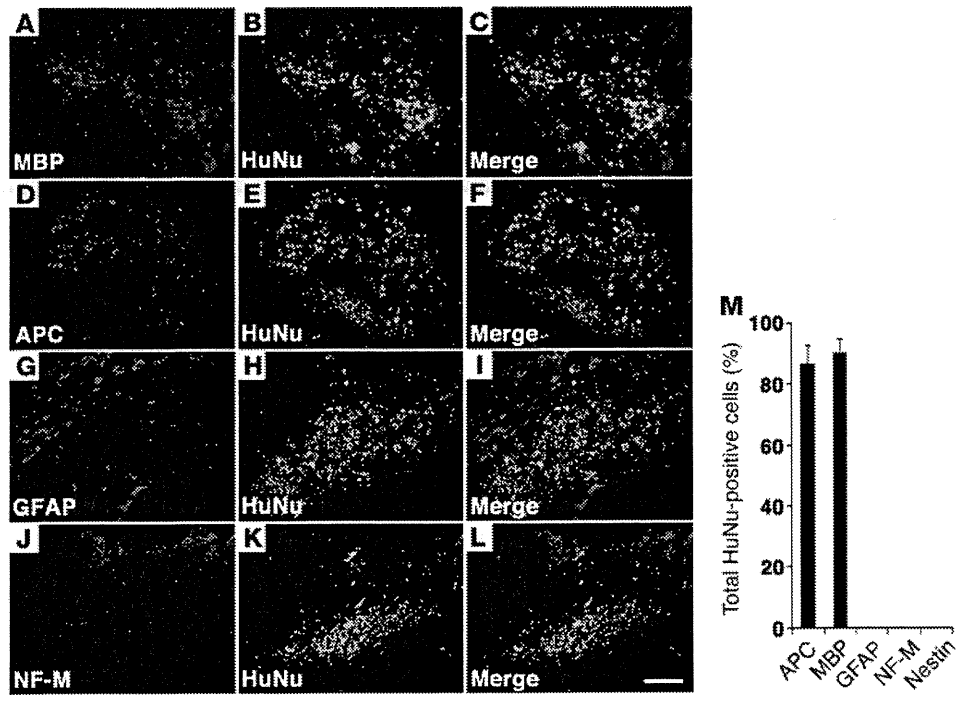

Figure 7
SHEDs differentiate into mature oligodendrocytes in the transected SC. A myelin-positive cell cluster ectopically identified in the medulla of a SHED-transplanted SC (boxed area in Figure 6B) was characterized by immunohistochemical staining with an anti–human nuclei mAb (HuNu) together with Abs against neural cell lineage markers: anti-MBP (**A**–**C**), anti-APC (**D**–**F**), anti-GFAP (**G**–**I**), or anti–NF-M (**J**–**L**). The data indicate that SHEDs specifically differentiate into mature oligodendrocytes. The percentage of the lineage marker–positive to total HuNu-positive cell number (**M**) represents the average of 3 experiments performed in parallel. Error bars represent SD. Scale bar: 100 μm (**L**).

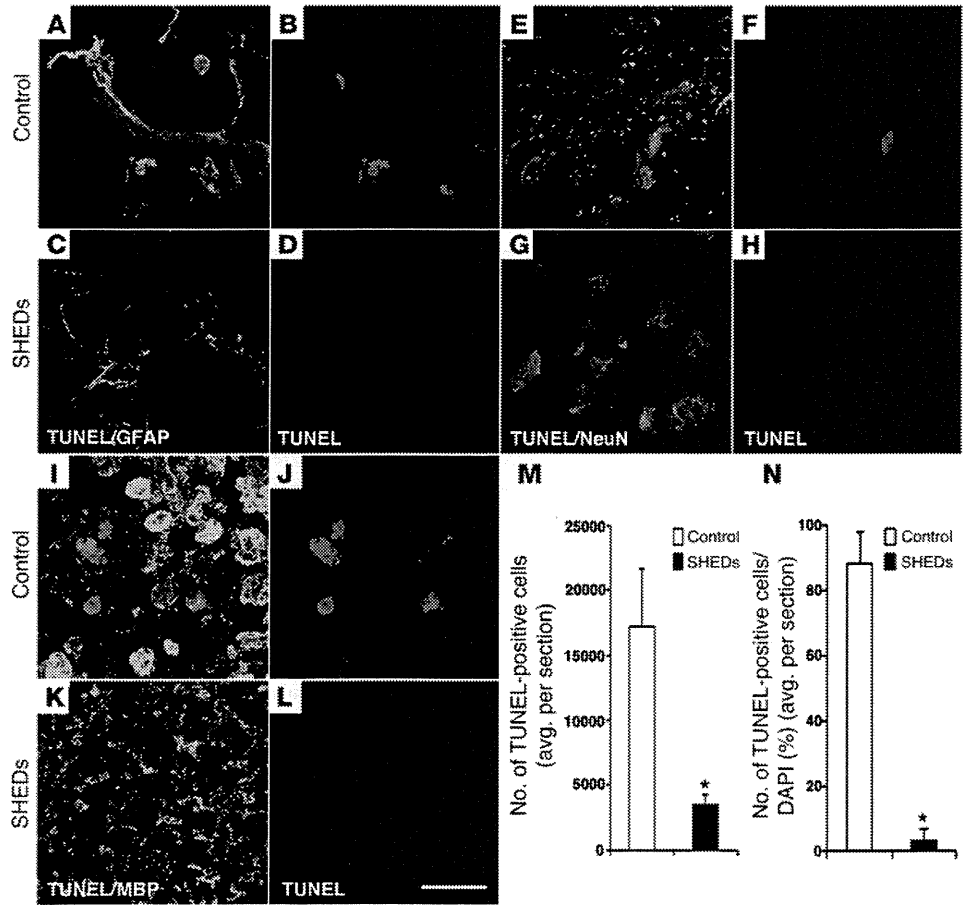

Figure 8
SHEDs suppress the apoptosis of neural cell lineages and secondary injury after SCI. Representative images (**A**–**L**) and quantifications (**M** and **N**) of apoptotic cell death 24 hours after SCI. Transverse sections 1 mm caudal to the epicenter of PBS-injected (**A**, **B**, **E**, **F**, **I**, and **J**) and SHED-transplanted SCs (**C**, **D**, **G**, **H**, **K**, and **L**) were stained with TUNEL and then subjected to immunohistochemical analysis with an anti-GFAP mAb (**A**–**D**), anti-NeuN mAb (**E**–**H**), or anti-MBP mAb (**I**–**L**). The engrafted SHEDs decreased the apoptotic cell death of all 3 neural cell lineages. (**M**) Quantification of the total TUNEL-positive cell number within 3 mm rostral and caudal to the epicenter shows the average of 3 experiments performed in parallel. (**N**) The percentage of TUNEL-positive relative to total DAPI-positive cell number in the same area as in **M**. Error bars represent SD. $^*P < 0.01$ compared with SCI models injected with PBS. Scale bar: 20 μm (**L**).

Methods

Isolation of SHEDs and DPSCs, and cell culture. Human SHEDs and DPSCs were isolated as described previously (16, 17). Briefly, exfoliated deciduous teeth (from individuals 6–12 years old) and adult third molars (18–30 years old) extracted for clinical purposes were collected. After separation of the crown and root, the dental pulp was isolated and then digested in a solution of 3 mg/ml collagenase type I and 4 mg/ml dispase for 1 hour at 37°C. Single-cell suspensions (1×10^4 to 2×10^4 cells/ml) were plated on culture dishes in DMEM supplemented with 10% fetal calf serum, then incubated at 37°C in 5% CO_2. Mesenchymal stem cells of three human bone marrow lines (hBMSCs, from individuals 20–22 years old) at passage 5 and three human skin-fibroblast lines (hFbs, 36–40-years old) at passage 5 were obtained from Lonza and the Health Science Research Resources Bank Japan, respectively.

Real-time PCR and microarray analysis. Total RNA was quantified by a spectrophotometer, and RNA integrity was checked on 1% agarose gels. RT reactions were carried out with Superscript III reverse transcriptase (Invitrogen) using 1 μg of total RNA in a 50 μl total reaction volume. Real-time PCR was performed using the THUNDERBIRD SYBR qPCR Mix (Toyobo) driven by the StepOnePlus Real-Time PCR System (Applied Biosystems). Primers were designed using DNADynamo (BlueTractorSoftware Ltd) and primer 3, as follows: *BDNF* forward (5′-GGGAAAAGGGAACAGGAAAA-3′), *BDNF* reverse (5′-AACAGACAGGATGGGCAGAA-3′), *GDNF* forward (5′-CGAACTCTTGCCCCTGACCT-3′), *GDNF* reverse (5′-ACAGCCACGACATCCCATAAC-3′), *CNTF* forward (5′-CCTTCTCTCTTCCTTGCTTTCTCTT-3′), *CNTF* reverse (5′-TGTCCCTGCTCCCACTCTCT-3′), *NT-3* forward (5′-TCAAAACGGGCAACTCTCCT-3′), *NT-3* reverse (5′-CTCGACAAGGCACACACACA-3′), *NGF* forward (5′-TTCCCTTGACACTGCCCTTC-3′), *NGF* reverse (5′-GATGATGACCGCTTGCTCCT-3′). Microarray experiments were carried out using a CodeLink Human Whole Genome Bioarray (Applied Microarrays Inc.) at Filgen Inc. The arrays were scanned using a GenePix4000B Array Scanner (Molecular Devices). The data were analyzed by using MicroArray Data Analysis Tool version 3.2 (Filgen Inc.) and deposited in the GEO database (accession GSE32403).

Flow cytometry analysis. For flow cytometry, 1×10^6 cells were incubated with FITC-conjugated primary mAbs against CD34, CD45, and CD11b and PE-conjugated against HLA-DR, CD105, CD73, and CD90 (BD Biosciences) at 4°C for 30 minutes and then washed twice with PBS containing 0.1% bovine serum albumin. The expression of intracellular markers was examined by indirect immunostaining. Cells were fixed with 4% (w/v) PFA for 5 minutes and permeabilized with 0.1% (v/v) Triton X-100 in PBS for 5 minutes. After blocking with 10% (v/v) goat serum for 30 minutes, the cells were incubated with primary Abs: anti-GFAP (mouse IgG, 1:500, Millipore), anti-βIII-tubulin (mouse IgG, 1:1,000, R&D Systems), anti-NeuN (mouse IgG, 1:100, Millipore), anti-CNPase (mouse IgG, 1:500, Millipore), anti-nestin (rabbit IgG, 1:500, Millipore), anti-DCX (guinea pig IgG, 1:500, Millipore), anti-APC (rabbit IgG, 1:300, Abcam), anti-MBP (rabbit IgG, 1:500, Abcam), anti-A2B5 mAb (mouse IgG, 1:500, Millipore). The secondary Abs were anti-mouse IgG, anti-rabbit IgG, and anti-guinea pig IgG-conjugated with Alexa Fluor 448 (Invitrogen), used at 1:1,000. Cell fluorescence was evaluated by flow cytometry using a FACSCalibur (BD Biosciences).

Animal model and surgical procedure. Adult female Sprague-Dawley rats were anesthetized with a mixture of xylazine (100–150 mg/kg) and ketamine (60–90 mg/kg). After laminectomy at the 9th–11th thoracic vertebral lev-

els, the dura was opened, and the SC was completely transected using a surgical blade (Feather surgical blade stainless steel no. 11). The severed ends of the SCs typically retracted about 1–2 mm. The rostral and caudal stumps were lifted to ensure complete transection. Then, 1×10^6 cells were drawn into a glass pipette with a tip diameter of 50–70 mm mounted onto a 10-μl Hamilton syringe attached to a micromanipulator. First, the cells were deposited into two injection sites at the rostral and the caudal stumps, 2 mm from the lesion and 0.5 mm lateral to the midline, at a depth of 1.5 mm. A 2.5-μl sample containing 2.5×10^5 cells in PBS was grafted into each site (injection rate, 0.8 μl/min). Next, 1×10^5 cells in fibrin glue were implanted into the 1- to 2-mm gap to fill the lesion site in the severed SC. After surgery, the rats were placed in temperature- and humidity-controlled incubation chambers until they awoke. They were then transferred to cages, and bladder evacuation was applied daily. Antibiotics (sodium ampicillin, 10 mg/kg body weight) were injected into the rats daily for a week. The rats were maintained under postoperative care for 8 weeks. All rats were given cyclosporine (Novartis) at 10 mg/kg/d on the day before surgery transplantation, then every day after surgery.

Immunohistochemical analysis. Cells were plated on PLL-coated 8-chamber slides and then incubated with the primary Abs listed above. For histological examination of the treated SCs, the animals were anesthetized and transcardially perfused with 4% PFA in 0.1 M PBS, 8 weeks after transplantation. The SCs were embedded in OCT compound (Sakura Finetek) and sectioned in the sagittal or transverse plane at 20 μm on a cryostat (Leica). The sections were incubated with primary Abs against human nuclei (mouse IgG, 1:100), NF-M (rabbit IgG, 1:300, Millipore), and 5-HT (rabbit IgG, 1:500, Sigma-Aldrich) in addition to the Abs listed above. Secondary Abs were anti-mouse IgG–Alexa Fluor 488, anti-rabbit IgG–Alexa 546, and anti-guinea pig IgG–Alexa 647. Myelin was stained by FluoroMyelin green dye (Invitrogen), according to the manufacturer's instructions. After counterstaining with DAPI (Sigma-Aldrich), cell images were captured with a confocal laser scanning microscope (A1Rsi, Nikon), while tissue images were taken with a universal fluorescence microscope (BZ9000, Keyence).

The differentiation activity of the engrafted SHEDs and the cells staining positive for MBP, APC, NF-M, or GFAP among the anti-human nuclei–positive transplanted cells were quantified. Cells were counted in at least 15 confocal images from 3 individuals in parallel experiments, with error bars representing SD.

Anterograde neuronal tracing study. For tracing of the CSTs, 0.5 μl of 5% biotinylated dextran amine (BDA: MW 10,000, Molecular Probes, Invitrogen; 5% in PBS) was injected into 4 sites in the hind limb area of the sensorimotor cortex at a 1.2-mm depth, following the rat brain atlas (54). Two weeks after the injections, sagittal cryosections (20 μm thick) of the SCs were prepared and processed by diaminobenzidine (DAB) staining with the ABC reaction protocol (VECTASTAIN Elite ABC, Vector Laboratories).

BBB open field locomotor score. Hind limb neurobehavioral testing was performed using the BBB locomotor rating scale (24). The 22-point (from 0 to 21) BBB scale was used to assess hind limb locomotor recovery, including joint movements, stepping ability, coordination, and trunk stability. A score of 21 indicates unimpaired locomotion as observed in uninjured rats. Two examiners who were blinded to the animal's treatments performed the tests. The duration of each session was 4 minutes per rat. The scores were analyzed by repeated-measures ANOVA with Tukey's multiple comparison tests at each time point.

CM. At 70%–80% confluence, the cell culture medium was changed to serum-free DMEM. After 48 hours incubation at 37°C in 5% CO_2, the CM was collected and centrifuged for 4–5 minutes at 4°C, 22,140 *g*. After the brief re-centrifugation, the supernatant was collected and used as CM.

Neurite outgrowth assays. Forty-eight-well tissue culture plates (Falcon, BD) were coated with 20 μg/ml PLL (Sigma-Aldrich) and then with 300 ng/ml extracellular CSPG mixture (Millipore) or 400 ng/ml MAG/Fc Chimera (MAG; Sigma-Aldrich) for 4 hours at 37°C. Rat CGNs were seeded onto PLL-, PLL/CSPG-, or PLL/MAG-coated 48-well tissue culture plates at 2.0×10^4 cells/well and cultured at 37°C in 5% CO_2 with SHED-CM, DPSC-CM, BMSC-CM, or fibroblast-CM. After 24 hours incubation, cells were fixed in 4% paraformaldehyde/PBS and stained with anti-neuron-specific βIII-tubulin (R&D Systems) to visualize neurites. Cell processes were defined as neurites when they were longer than the diameter of the cell body. Neurite length was evaluated by manually tracing neurite per cell using ImageJ software (version 1.29, http://rsbweb.nih.gov/ij/) and referenced to a known length. Each experiment was conducted in triplicate, and images were taken with 20 or more cells per field. For each experiment, at least 100 cells were randomly counted and measured.

Analysis of apoptosis. Apoptotic cell death was analyzed by TUNEL assay (In Situ Cell Death Detection kit, Roche). TUNEL-positive cells were counted on sections from sham-treated, PBS-injected, and SHED-transplanted animals. A researcher blinded to the experimental protocol determined the number of TUNEL-positive cells in the entire serial parasagittal section. The average number of TUNEL-positive cells per section was calculated from the values obtained by counting serial sagittal sections through the lesion site of each animal, with 3 animals examined per group.

Statistics. An unpaired 2-tailed Student's *t* test was used for single comparisons. For analysis of the real-time PCR results and open-field scores, we used repeated-measures ANOVA with Tukey's post hoc test (SPSS 19.0). A *P* value less than 0.05 was considered significant.

Study approval. The animal studies were carried out in accordance with the NIH Guidelines for the Care and Use of Laboratory Animals and approved by the Animal Research Committee of Nagoya University. Extracted teeth were collected at the Nagoya University School of Medicine, under approved guidelines set by Nagoya University (H-73, 2003). Ethical approval was obtained from the ethics committee of Nagoya University (permission number 8-2). All participants provided written informed consent.

Acknowledgments

We are grateful to T. Yamashita (Osaka University) and M. Hibi (Nagoya University) for critical reading of the manuscript. We also thank T. Isa and T. Umeda (National Institute for Physiological Sciences); M. Koda and H. Takahashi (Chiba University); and M. Abematsu (Kagoshima University) for technical instruction. We are grateful to M. Fujio and R. Shohara for their comments and support of this study. We thank the Division of Experimental Animals and Medical Research Engineering, Nagoya University Graduate School of Medicine, for the housing of mice and for microscope maintenance. This work was supported by Grants-in-Aid for Scientific Research on Priority Areas from the Ministry of Education, Culture, Sports, Science and Technology of Japan; Grants-in-Aid for Practical Application of Regenerative Medicine from the Ministry of Health, Labour and Welfare of Japan; and COE for education and research of Micro-Nano Mechatronics Nagoya University Global COE Program.

Received for publication May 31, 2011, and accepted in revised form October 12, 2011.

Address correspondence to: Akihito Yamamoto, Department of Oral and Maxillofacial Surgery, Nagoya University Graduate School of Medicine, 65 Tsurumai-cho, Showa-ku, Nagoya 466-8550, Japan. Phone: 81.52.744.1978; Fax: 81.52.744.1978; E-mail: akihito@med.nagoya-u.ac.jp.

1. Norenberg MD, Smith J, Marcillo A. The pathology of human spinal cord injury: defining the problems. *J Neurotrauma.* 2004;21(4):429–440.
2. Schwab JM, et al. Experimental strategies to promote spinal cord regeneration — an integrative perspective. *Prog Neurobiol.* 2006;78(2):91–116.
3. Rowland JW, Hawryluk GW, Kwon B, Fehlings MG. Current status of acute spinal cord injury pathophysiology and emerging therapies: promise on the horizon. *Neurosurg Focus.* 2008;25(5):E2.
4. Yiu G, He Z. Glial inhibition of CNS axon regeneration. *Nat Rev Neurosci.* 2006;7(8):617–627.
5. Cummings BJ, et al. Human neural stem cells differentiate and promote locomotor recovery in spinal cord-injured mice. *Proc Natl Acad Sci U S A.* 2005; 102(39):14069–14074.
6. Keirstead H, et al. Human embryonic stem cell-derived oligodendrocyte progenitor cell transplants remyelinate and restore locomotion after spinal cord injury. *J Neurosci.* 2005;25(19):4694–4705.
7. Kumagai G, et al. Roles of ES cell-derived gliogenic neural stem/progenitor cells in functional recovery after spinal cord injury. *PLoS One.* 2009;4(11):e7706.
8. Erceg S, et al. Transplanted oligodendrocytes and motoneuron progenitors generated from human embryonic stem cells promote locomotor recovery after spinal cord transection. *Stem Cells.* 2010; 28(9):1541–1549.
9. Hofstetter CP, et al. Marrow stromal cells form guiding strands in the injured spinal cord and promote recovery. *Proc Natl Acad Sci U S A.* 2002; 99(4):2199–2204.
10. Cizkova D, Rosocha J, Vanicky I, Jergova S, Cizek M. Transplants of human mesenchymal stem cells improve functional recovery after spinal cord injury in the rat. *Cell Mol Neurobiol.* 2006; 26(7–8):1167–1180.
11. Sharp J, Keirstead HS. Therapeutic applications of oligodendrocyte precursors derived from human embryonic stem cells. *Curr Opin Biotechnol.* 2007; 18(5):434–440.
12. Deshpande DM, et al. Recovery from paralysis in adult rats using embryonic stem cells. *Ann Neurol.* 2006;60(1):32–44.
13. Kopen GC, Prockop DJ, Phinney DG. Marrow stromal cells migrate throughout forebrain and cerebellum, and they differentiate into astrocytes after injection into neonatal mouse brains. *Proc Natl Acad Sci U S A.* 1999;96(19):10711–10716.
14. Furuya T, et al. Treatment of rat spinal cord injury with a Rho-kinase inhibitor and bone marrow stromal cell transplantation. *Brain Res.* 2009; 1295:192–202.
15. Gronthos S, et al. Stem cell properties of human dental pulp stem cells. *J Dent Res.* 2002;81(8):531–535.
16. Gronthos S, Mankani M, Brahim J, Robey PG, Shi S. Postnatal human dental pulp stem cells (DPSCs) in vitro and in vivo. *Proc Natl Acad Sci U S A.* 2000;97(25):13625–13630.
17. Miura M, et al. SHED: stem cells from human exfoliated deciduous teeth. *Proc Natl Acad Sci U S A.* 2003;100(10):5807–5812.
18. Arthur A, Rychkov G, Shi S, Koblar SA, Gronthos S. Adult human dental pulp stem cells differentiate toward functionally active neurons under appropriate environmental cues. *Stem Cells.* 2008; 26(7):1787–1795.
19. Wang J, et al. Stem cells from human-exfoliated deciduous teeth can differentiate into dopaminergic neuron-like cells. *Stem Cells Dev.* 2010; 19(9):1375–1383.
20. Nosrat IV, Widenfalk J, Olson L, Nosrat CA. Dental pulp cells produce neurotrophic factors, interact with trigeminal neurons in vitro, and rescue motoneurons after spinal cord injury. *Dev Biol.* 2001; 238(1):120–132.
21. Nosrat IV, Smith CA, Mullally P, Olson L, Nosrat CA. Dental pulp cells provide neurotrophic support for dopaminergic neurons and differentiate into neurons in vitro; implications for tissue engineering and repair in the nervous system. *Eur J Neurosci.* 2004;19(9):2388–2398.
22. Huang AH-C, Snyder BR, Cheng P-H, Chan AWS. Putative dental pulp-derived stem/stromal cells promote proliferation and differentiation of endogenous neural cells in the hippocampus of mice. *Stem Cells.* 2008;26(10):2654–2663.
23. Arthur A, Shi S, Zannettino AC, Fujii N, Gronthos S, Koblar SA. Implanted adult human dental pulp stem cells induce endogenous axon guidance. *Stem Cells.* 2009;27(9):2229–2237.
24. Basso DM, Beattie MS, Bresnahan JC. A sensitive and reliable locomotor rating scale for open field testing in rats. *J Neurotrauma.* 1995;12(1):1–21.
25. Mirsky R, Winter J, Abney ER, Pruss RM, Gavrilovic J, Raff MC. Myelin-specific proteins and glycolipids in rat Schwann cells and oligodendrocytes in culture. *J Cell Biol.* 1980;84(3):483–494.
26. Bhat RV, et al. Expression of the APC tumor suppressor protein in oligodendroglia. *Glia.* 1996; 17(2):169–174.
27. In 't Anker PS, et al. Isolation of mesenchymal stem cells of fetal or maternal origin from human placenta. *Stem Cells.* 2004;22(7):1338–1345.
28. Romanov YA, Svintsitskaya VA, Smirnov VN. Searching for alternative sources of postnatal human mesenchymal stem cells: candidate MSC-like cells from umbilical cord. *Stem Cells.* 2003; 21(1):105–110.
29. Young HE, et al. Human reserve pluripotent mesenchymal stem cells are present in the connective tissues of skeletal muscle and dermis derived from fetal, adult, and geriatric donors. *Anat Rec.* 2001; 264(1):51–62.
30. Zuk PA, et al. Human adipose tissue is a source of multipotent stem cells. *Mol Biol Cell.* 2002; 13(12):4279–4295.
31. Nombela-Arrieta C, Ritz J, Silberstein LE. The elusive nature and function of mesenchymal stem cells. *Nat Rev Mol Cell Biol.* 2011;12(2):126–131.
32. Maekawa M, et al. Signaling from Rho to the actin cytoskeleton through protein kinases ROCK and LIM-kinase. *Science.* 1999;285(5429):895–898.
33. Winton MJ, Dubreuil CI, Lasko D, Leclerc N, McKerracher L. Characterization of new cell permeable C3-like proteins that inactivate Rho and stimulate neurite outgrowth on inhibitory substrates. *J Biol Chem.* 2002;277(36):32820–32829.
34. Yamashita T, Tohyama M. The p75 receptor acts as a displacement factor that releases Rho from Rho-GDI. *Nat Neurosci.* 2003;6(5):461–467.
35. Monnier PP, Sierra A, Schwab JM, Henke-Fahle S, Mueller BK. The Rho/ROCK pathway mediates neurite growth-inhibitory activity associated with the chondroitin sulfate proteoglycans of the CNS glial scar. *Mol Cell Neurosci.* 2003;22(3):319–330.
36. Dubreuil C, Winton M, McKerracher L. Rho activation patterns after spinal cord injury and the role of activated Rho in apoptosis in the central nervous system. *J Cell Biol.* 2003;162(2):233–243.
37. Hall A. Rho GTPases and the actin cytoskeleton. *Science.* 1998;279(5350):509–514.
38. Lehmann M, et al. Inactivation of Rho signaling pathway promotes CNS axon regeneration. *J Neurosci.* 1999;19(17):7537–7547.
39. Dergham P, Ellezam B, Essagian C, Avedissian H, Lubell WD, McKerracher L. Rho signaling pathway targeted to promote spinal cord repair. *J Neurosci.* 2002; 22(15):6570–6577.
40. Fournier AE, Takizawa BT, Strittmatter SM. Rho kinase inhibition enhances axonal regeneration in the injured CNS. *J Neurosci.* 2003;23(4):1416–1423.
41. Celik M, et al. Erythropoietin prevents motor neuron apoptosis and neurologic disability in experimental spinal cord ischemic injury. *Proc Natl Acad Sci U S A.* 2002;99(4):2258–2263.
42. Gorio A, et al. Recombinant human erythropoietin counteracts secondary injury and markedly enhances neurological recovery from experimental spinal cord trauma. *Proc Natl Acad Sci U S A.* 2002; 99(14):9450–9455.
43. Wang X, et al. P2X7 receptor inhibition improves recovery after spinal cord injury. *Nature Med.* 2004; 10(8):821–827.
44. Demjen D, et al. Neutralization of CD95 ligand promotes regeneration and functional recovery after spinal cord injury. *Nature Med.* 2004;10(4):389–395.
45. Stirling DP, et al. Minocycline treatment reduces delayed oligodendrocyte death, attenuates axonal dieback, and improves functional outcome after spinal cord injury. *J Neurosci.* 2004;24(9):2182–2190.
46. Teng YD, et al. Minocycline inhibits contusion-triggered mitochondrial cytochrome c release and mitigates functional deficits after spinal cord injury. *Proc Natl Acad Sci U S A.* 2004;101(9):3071–3076.
47. Bush TG, et al. Leukocyte infiltration, neuronal degeneration, and neurite outgrowth after ablation of scar-forming, reactive astrocytes in adult transgenic mice. *Neuron.* 1999;23(2):297–308.
48. Faulkner JR, Herrmann JE, Woo MJ, Tansey KE, Doan NB, Sofroniew MV. Reactive astrocytes protect tissue and preserve function after spinal cord injury. *J Neurosci.* 2004;24(9):2143–2155.
49. Okada S, et al. Conditional ablation of Stat3 or Socs3 discloses a dual role for reactive astrocytes after spinal cord injury. *Nature Med.* 2006; 12(7):829–834.
50. Herrmann JE, et al. STAT3 is a critical regulator of astrogliosis and scar formation after spinal cord injury. *J Neurosci.* 2008;28(28):7231–7243.
51. Rolls A, Shechter R, Schwartz M. The bright side of the glial scar in CNS repair. *Nat Rev Neurosci.* 2009;10(3):235–241.
52. Keirstead HS. Stem cells for the treatment of myelin loss. *Trends Neurosci.* 2005;28(12):677–683.
53. Thuret S, Moon LDF, Gage FH. Therapeutic interventions after spinal cord injury. *Nat Rev Neurosci.* 2006;7(8):628–643.
54. Paxinos G, Watson C. *The Rat Brain in Stereotaxic Coordinates.* 2nd ed. Orlando, Florida, USA: Academic Press; 1986.

Journal of Bioscience and Bioengineering
VOL. 111 No. 3, 255-258, 2011

ELSEVIER

www.elsevier.com/locate/jbiosc

NOTE

Gingival and dermal fibroblasts: Their similarities and differences revealed from gene expression

Katsumi Ebisawa,[1,2,†] Ryuji Kato,[3,4,†] Mai Okada,[3,4,5] Tomotaka Sugimura,[3] Mazlyzam Abdul Latif,[5,6] Yusuke Hori,[7] Yuji Narita,[3,5,8] Minoru Ueda,[1] Hiroyuki Honda,[4] and Hideaki Kagami[5,9,*]

Department of Oral and Maxillofacial Surgery, Nagoya University Graduate School of Medicine, 65 Tsuruma-cho, Showa-ku, Nagoya 466-8550, Japan,[1] Department of Plastic and Reconstructive Surgery, Nagoya University Graduate School of Medicine, 65 Tsuruma-cho, Showa-ku, Nagoya 466-8550, Japan,[2] Department of Clinical Cell Therapy, Nagoya University School of Medicine, 65 Tsuruma-cho, Showa-ku, Nagoya 466-8550, Japan,[3] Department of Biotechnology, Graduate School of Engineering, Nagoya University, Furo-cho, Chikusa-ku, Nagoya 464-8603, Japan,[4] Department of Tissue Engineering, Nagoya University School of Medicine, 65 Tsuruma-cho, Showa-ku, Nagoya 466-8550, Japan,[5] Department of Biomedical Science, Faculty of Allied Health Sciences, Universiti Kebangsaan Malaysia, Jalan Raja Muda Abdul Aziz, 50300 Kuala Lumpur, Malaysia,[6] Education Center for Integrative Medicine, Nihon Pharmaceutical University, 10281 Komuro, Ina-cho, Kitaadachi-gun, Saitama 362-0806, Japan,[7] Department of Cardiac Surgery, Nagoya University Graduate School of Medicine, 65 Tsuruma-cho, Showa-ku, Nagoya 466-8550, Japan,[8] and Division of Molecular Therapy, The Institute of Medical Science, The University of Tokyo, 4-6-1 Shirokanedai, Minato-ku, Tokyo 108-8639, Japan[9]

Received 3 June 2010; accepted 18 November 2010
Available online 1 February 2011

Gene expression profiles in normal human gingival and dermal fibroblasts were investigated using DNA microarrays. Their fundamental characteristics were almost identical, but 5% of their genes were uniquely expressed. These results help us to choose an optimal cell source for effective fibroblast-based cell therapy that is dependent on differential gene expression profiles.

[**Key words:** Fibroblast; Gingival tissue; Anti-aging; Microarray; Antioxidant]

Fibroblasts are widely used for regenerative medicine in clinics, such as gingival (1) or facial skin treatment (2). In fact, fibroblasts are considered to be a mixture of various types of cells of "spindle shape" and as such there are no clearly defined biomarkers of fibroblasts. Gingival and dermal fibroblasts are similar in their morphology and function. However, it is considered that cultured cells retain the original characteristics of the tissue of origin and therefore may induce differential therapeutic effects. For example, gingival wounds are known to heal relatively quickly with less scar formation compared with skin wounds, which may imply that gingival fibroblasts have a higher capability for regeneration in cell-based therapies (3). The reason for this phenomenon may be partly due to characteristic differences between gingival and dermal fibroblasts including the expression of migration stimulating factor (4) and matrix formation (5) but these differences remain largely unknown. Recently, the characteristics of dermal fibroblasts have been reported to be different depending on the skin source, such as face, trunk and palmoplantar skin (6). Although the expression of fibronectin and its alternative splice variants are known to be different between trunk and oral mucosal fibroblasts, there is still no detailed report on the functional differences between gingival and dermal fibroblasts (7). In this study, we investigated differential gene expression in normal gingival and dermal fibroblasts using DNA microarray to investigate the difference between the vague fibroblast-type cells from different tissue origin to achieve higher therapeutic effect in cell therapy.

This study conformed to the tenets of the Declaration of Helsinki. Dermal and oral tissues were obtained from healthy volunteers (8 cases of facial skin from the postauricular crease: 5 females, 3 males, average age 48, and 8 cases of oral mucosa from the posterior vestibule: 6 females, 2 males, average age 43) whose informed consent was obtained according to a protocol approved by the ethics committee of Nagoya University Hospital. After enzymatic digestion, dermal and mucosal fibroblasts were cultured in Dulbecco's modified Eagle's medium (DMEM) containing 10% fetal bovine serum at 37°C in the presence of 5% CO_2 for about 4 weeks as reported previously (8). Total mRNAs were extracted from cells between passages 4–5 by Trizol reagent (Invitrogen, Carlsbad, CA, USA) and were applied to Human Focus Arrays (Affymetrix, Santa Clara, CA, USA) for microarray analysis according to the manufacturer's protocol (http://www.affymetrix.com/support/technical/manuals.affx). The gene expression data were analyzed by Arrayassist (Stratagene, La Jolla, CA, USA).

* Corresponding author. Division of Molecular Therapy, The Institute of Medical Science, The University of Tokyo, 4-6-1 Shirokanedai, Minato-ku, Tokyo 108-8639, Japan. Tel.: +81 3 5449 5120; fax: +81 3 5449 5121.
E-mail address: kagami@ims.u-tokyo.ac.jp (H. Kagami).
† K. E. and R. K. contributed equally to this project.

1389-1723/$ - see front matter
doi:10.1016/j.jbiosc.2010.11.014

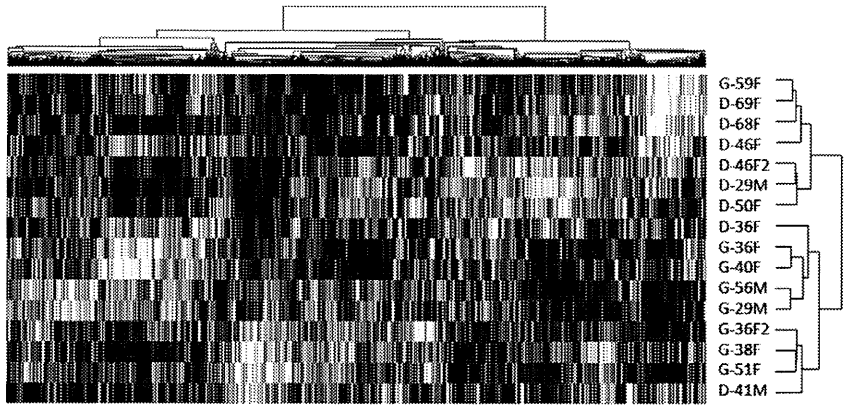

FIG. 1. Hierarchical clustering of 5284 genes comparing gingival and dermal fibroblasts (8 clinical samples were collected for each tissue origin). Samples are designated by tissue origin (G; gingival/D; dermal) followed by ages and sex (M; male/F; female). Rows, samples; columns, genes. White, highly expressed in dermal fibroblasts (>0.8); Black, highly expressed in gingival fibroblasts (−1.0), intermediate colors represents the gradient between white and black.

Briefly, 8500 probes on the array, normalization and scaling (MAS5), flag-positive gene selection, unpaired *t*-test, and CV selection (<20) resulted in 5284 genes to analyze (GEO accession number: GSE22029). GO (Gene ontology) analysis was performed using the software default settings to find the gene group related to the same category of biological function by searching common key terms that were reported for each gene.

From comparison of expression profiles of 5284 genes in dermal and gingival fibroblasts, only 5% (278 genes) showed a significant difference in the levels of expression after noise reduction. These results and the GO analysis indicated that the fundamental characteristics of both dermal and gingival fibroblasts were almost identical. On the other hand, among 278 genes, 164 and 114 genes were uniquely expressed in gingival and dermal fibroblasts, respectively. Interestingly, the number and fold differences of those uniquely expressed genes were more evident in gingival fibroblasts. Hierarchical clustering of total genes showed that the difference between gingival and dermal fibroblasts was larger than the difference between ages or gender of patients (Fig. 1). This indicates that gingival and dermal fibroblasts retain most of their functions in common, although there were some genes that specifically characterized each fibroblast type. Table 1 indicates representative GO hierarchies, which showed significant fold differences. Major differences were observed in extracellular matrix-related genes, oxidoreductase activity-related genes, cytokine activity-related genes and growth factor-related genes.

TABLE 1. Gene list from microarray analysis of gingival fibroblasts and dermal fibroblasts.

GO hierarchy	Gene title	Probe set ID	*p*-value	Tissue specificity	Fold change
Aging	T-box 2	40560_at	0.002	gingival	2.68
Odioreductase activity	hydroxysteroid (17-beta) dehydrogenase 2	204818_at	0.000	gingival	15.69
	dehydrogenase/reductase (SDR family) member 3	202481_at	0.000	gingival	5.45
	aldo-keto reductase family 1, member B10 (aldose reductase)	206561_s_at	0.002	gingival	4.31
	superoxide dismutase 3, extracellular	205236_x_at	0.004	gingival	3.97
	lectin, galactoside-binding, soluble, 3 binding protein	200923_at	0.000	gingival	3.38
	cytochrome P450, family 26, subfamily B, polypeptide 1	219825_at	0.010	dermal	6.69
	prostaglandin-endoperoxide synthase 1	215813_s_at	0.003	dermal	3.12
Antioxidant activity	superoxide dismutase 3, extracellular	205236_x_at	0.004	gingival	3.97
	prostaglandin-endoperoxide synthase 1	215813_s_at	0.003	dermal	3.12
Extracellular matrix	glypican 3	209220_at	0.001	gingival	13.29
	collagen, type IV, alpha 1	211980_at	0.000	gingival	4.24
	superoxide dismutase 3, extracellular	205236_x_at	0.004	gingival	3.97
	lectin, galactoside-binding, soluble, 3 binding protein	200923_at	0.000	gingival	3.38
	matrix metallopeptidase 12 (macrophage elastase)	204580_at	0.003	dermal	25.54
	tenascin C (hexabrachion)	201645_at	0.006	dermal	6.56
	collagen, type X, alpha 1 (Schmid metaphyseal chondrodysplasia)	217428_s_at	0.005	dermal	3.86
Cytokine activity	chemokine (C-X-C motif) ligand 14	218002_s_at	0.009	gingival	8.20
	platelet-derived growth factor alpha polypeptide	205463_s_at	0.001	gingival	6.21
	tumor necrosis factor (ligand) superfamily, member 10	202688_at	0.007	gingival	5.81
	chemokine (C-X-C motif) ligand 12 (stromal cell-derived factor 1)	203666_at	0.007	gingival	4.01
	midkine (neurite growth-promoting factor 2)	209035_at	0.002	gingival	3.07
	cytochrome P450, family 26, subfamily B, polypeptide 1	219825_at	0.010	dermal	6.69
Growth factor activity	insulin-like growth factor 2 (somatomedin A)	202409_at	0.003	gingival	21.88
	platelet-derived growth factor alpha polypeptide	205463_s_at	0.001	gingival	6.21
	chemokine (C-X-C motif) ligand 12 (stromal cell-derived factor 1)	203666_at	0.007	gingival	4.01
	jagged 1 (Alagille syndrome)	216268_s_at	0.004	gingival	3.33
	placental growth factor, vascular endothelial growth factor-related protein	209652_s_at	0.007	gingival	3.09
	midkine (neurite growth-promoting factor 2)	209035_at	0.002	gingival	3.07
Insulin related	insulin-like growth factor 2 (somatomedin A) /// insulin-insulin-like growth factor	202409_at	0.003	gingival	21.88
	insulin-like growth factor binding protein 4	201508_at	0.010	gingival	2.00
	insulin-like growth factor binding protein 6	203851_at	0.010	gingival	2.42
Angiogenesis related	endothelial differentiation, sphingolipid G-protein-coupled receptor, 1	204642_at	0.002	gingival	3.61
	endothelial differentiation, lysophosphatidic acid G-protein-coupled receptor, 7	220816_at	0.005	dermal	4.56

In terms of differential gene expression of different sources of fibroblasts, the results from subtracted cDNA libraries have been reported (7). Higher expression of fibronectin mRNA was noted in trunk skin fibroblasts than in sole skin or oral mucosal fibroblasts. This finding was confirmed at the protein level and fibronectin and integrins (α5, αV, β1 and β3) were expressed more abundantly in fibroblasts derived from trunk skin than those derived from sole skin or oral mucosa. The results from a more comprehensive analysis were also reported using cultured fetal and adult human fibroblasts derived from different anatomical sites using DNA microarrays (6). Distinct and characteristic transcriptional patterns were reported for genes related to extracellular matrix production (*MMP9, ADAM12, lysyl oxidase, fibronectin 1, fibrillin 1, ADAMTS-like 1, thrombospondin 2, COL6A1, discoidin domain receptor 1, COL4A6, COL5A3, lysine hydroxylase, COL1A1, COL4A1, COL4A2,* and *PCOLCE2*), genes related to cell fate determination and inductive interactions (*FOXF, 1FOXP1, HGF, BMP4, FLT1,* and *FGF7*), genes related to growth and differentiation signaling molecules (*transforming growth factor, BMP4, inhibin, follistatin, Wnt2, Wnt5, frizzled homologs 1, 4, and 8, WISP2, DAAM2, GPRC1, GPRC48, FGF18, neuregulin, insulin-like growth factor 2, connective tissue growth factor, IGFBP7, IGFBF2, PTPRC,* and *PTPRM*), and genes related to cell migration signals (*SEMA3F, SEMA3C, neuropilin 2, plexin C1, SLIT2, SLIT3, ephrin B2, F-spondin, midkine,* and *pleiotrophin*). However, differential gene expression profiles between gingival and skin fibroblasts were not particularly discussed.

In this study, genes preferentially expressed in gingival fibroblasts included *Insulin like growth factor 2* (IGF-2) ($p<0.03$, fold change (FC)>21.9), *hydroxysteroid (17-beta) dehydrogenase 2* ($p<0.001$, FC>15.7), and *glypican 3* ($p<0.001$, FC>13.3). On the other hand, expression of *matrix metallopeptidase 12* (macrophage elastase) was more evident in dermal fibroblasts ($p<0.003$, FC>25.5) than gingival fibroblasts. Studies suggest that IGF-2, which is preferentially expressed in gingival fibroblasts, is known to play a key role in mammalian growth, influencing fetal cell division and differentiation and possibly metabolic regulation (9). Compared with *insulin-like growth factor 1*, which plays important roles in physiological regulation in adults, IGF-2 is considered as a growth factor that is highly active during fetal development but less active in the adult. Although the function of IGF-2 in gingival fibroblasts remains to be elucidated, IGFs have been reported to exert autocrine and paracrine effects on proliferation, migration and survival of fibroblasts (10). Since this factor is highly expressed in gingival fibroblasts, it may explain, at least in part, the characteristic features of oral mucosa. *Matrix metallopeptidase 12*, which is preferentially expressed in dermal fibroblasts, belongs to the matrix metalloproteinase (MMP) family and is involved in the breakdown of extracellular matrix in normal physiological processes such as embryonic development, reproduction, and tissue remodeling as well as in many disease processes such as arthritis and aneurysms (11). Accordingly, higher MMP expression might be beneficial for the treatment of scar tissue, which requires tissue remodeling of excessive fibrous tissue and matrices. Another interesting finding includes the higher expression of *superoxide dismutase 3* in gingival fibroblasts ($p<0.025$, FC>3.97). Superoxide dismutases (SOD) are a class of enzymes that catalyze the dismutation of superoxide into oxygen and hydrogen peroxide. Accordingly, they are considered as part of a defense system for oxidative stress in most cell types. The role of SOD in gingival fibroblasts is not clear but oral mucosa is ordinarily exposed to various noxious stimuli such as food and microorganisms in the environment, which can cause periodontitis. SOD may be protective from those stimuli (12). The higher expression of this enzyme in gingival fibroblasts may be beneficial to protect cells/tissues from oxidative

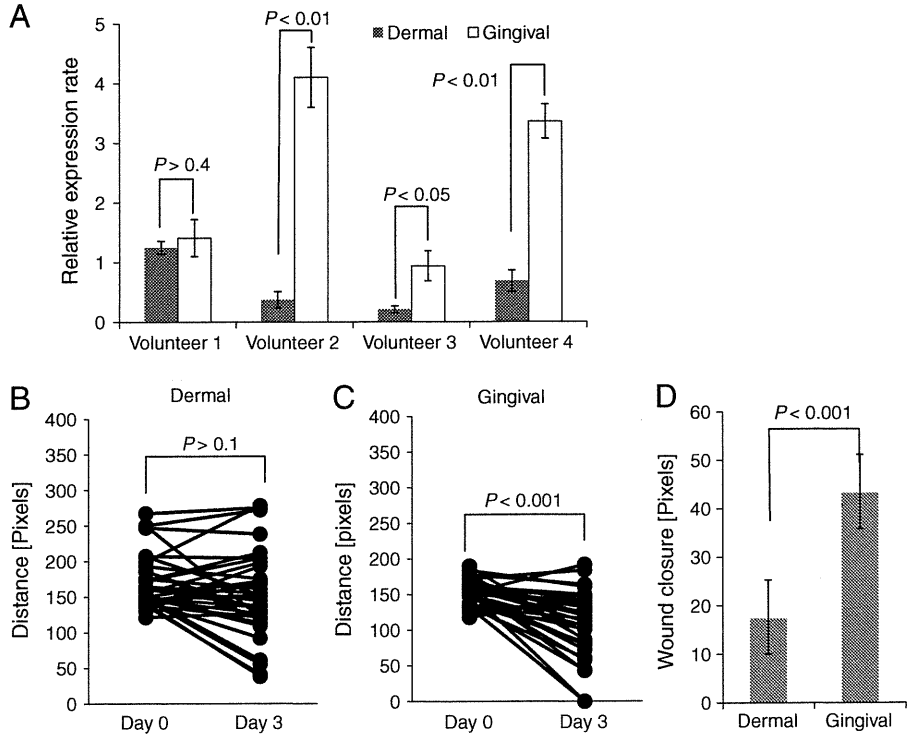

FIG. 2. The results from RT-PCR and scratch assay. The expression of *IGF-2* from dermal and gingival fibroblasts was analyzed. The level of *IGF-2* was significantly higher in gingival fibroblasts compared with dermal fibroblasts except in one volunteer, which confirmed the results of microarray analysis (A). Confluent keratinocytes were wounded with a 20 μl pipette tip and then treated with conditioned medium from dermal and gingival fibroblasts. The wound width was not significantly reduced from day 0 to day 3 in cells treated with the conditioned medium from dermal fibroblasts (B) but was reduced in cells treated with conditioned medium from gingival fibroblasts ($p<0.01$) (C). Wound closure (width change) from day 0 to day 3 was calculated and plotted as the mean ± SEM. In this model, wound closure was significantly accelerated when the cells were treated with conditioned medium from gingival fibroblasts than with conditioned medium from dermal fibroblasts ($p<0.01$) (D).

stress at the transplanted site. Recently, dermal fibroblast injections have been widely performed and are expected to increase collagen synthesis for the treatment of various facial contour defects and also as anti-aging treatments. Use of gingival fibroblasts may confer an additional effect via protection against anti-oxidative stress (13).

To confirm our microarray analysis data, we further investigated the expression of *IGF-2*, which was the most highly expressed gene in gingival fibroblasts compared to dermal fibroblasts. Gingival fibroblasts were obtained from additional 4 healthy volunteers (4 males, average age 26) as described above and the level of *IGF-2* expression was evaluated by RT-PCR with the primers (Forward: CTTGGACTTTGAGTCAAATTGG, Reverse: GGTCGTGCCAATTACATTTCA) under the PCR conditions of 94°C for 2 min (94°C for 30 s, 60°C for 30 s, 72°C for 30 s) ×35 cycles and 72°C for 10 min. The results were normalized to *beta-actin* expression using the primers (Forward: CCACACTGTGCCCATCTACG, Reverse: AGGATCTTCATGAGGTAGTCAGTCAG) under the PCR conditions of 95°C for 12 min (95°C for 30 s, 60°C for 1 min, 72°C for 1 min) ×40 cycles and 72°C for 1 min. *IGF-2* was significantly upregulated in three out of four volunteer's gingival fibroblasts compared to dermal fibroblasts (Fig. 2A), which confirmed the results of the microarray analysis.

To understand the functional aspects of differential gene expression profiles between gingival and dermal fibroblasts, a scratch assay was performed (Fig. 2B, C, D). Human epidermal keratinocytes (Kurabo, Osaka, Japan) were seeded in 6-well plates (5700 cells/cm^2) and cultured in EpiLife-KG2 media (Kurabo). Confluent keratinocytes on the bottom of wells ($N=3$) were wounded with a 20 μl pipette tip and then treated with conditioned medium (DMEM with 10% FBS) from either dermal or gingival fibroblast cultures from a healthy volunteer (male, age 25). Phase contrast microscopic images of crossed scratch positions ($N=12$ in each three wells) were obtained by Metamorph (Molecular Devices, Sunnyvale, CA, USA) with an electronically controlled stage at day 0 and day 3. The wound width was significantly reduced from day 0 to day 3 only with conditioned medium from gingival fibroblasts but not with conditioned medium from dermal fibroblasts (Fig. 2B, C). Wound closure (width change) was calculated by subtracting the width at day 3 from the width at day 0 (Fig. 2D). In this model, wound closure was significantly accelerated in the wells treated with conditioned medium from gingival fibroblasts than in wells treated with dermal fibroblast conditioned medium ($p<0.01$). Although the underlying mechanisms were not analyzed in this study, this data combined with the microarray analysis strongly suggests the presence of functional factor(s) in the conditioned medium that accelerate cell motility/growth of keratinocytes.

Although gene expression profiles of normal fibroblasts have been reported, as far as we could find, there is no detailed report on the differential gene expression between normal gingival and dermal fibroblasts. It is noteworthy that the unique characteristics of gingival and dermal fibroblasts reported here were found only by this direct and comprehensive comparison. Gene expression profiles from cultured and passaged cells may not be identical to those of the original tissues as shown for fibronectin (6), which means the results of this study do not necessarily reflect the characteristics of fibroblasts in tissues. However, the primary purpose of the present study was to understand the potential of therapeutic effects of cultured fibroblasts depending on their origin. These results should provide the possibility of effective treatment, which could be genetically designed to provide a higher therapeutic effect by selecting the origin of fibroblasts since gingival and dermal fibroblasts show some unique characteristics in their gene expression profiles.

References

1. **McGuire, M. K. and Nunn, M. E.:** Evaluation of the safety and efficacy of periodontal applications of a living tissue-engineered human fibroblast-derived dermal substitute: I. Comparison to the gingival autograft: a randomized controlled pilot study, J. Periodontol., **76**, 867–880 (2005).
2. **Watson, D., Keller, G. S., Lacombe, V., Fodor, P. B., Rawnsley, J., and Lask, G. P.:** Autologous fibroblasts for treatment of facial rhytids and dermal depressions. A pilot study, Arch. Facial Plast. Surg., **1**, 165–170 (1999).
3. **Eslami, A., Gallant-Behm, C. L., Hart, D. A., Wiebe, C., Honardoust, D., Gardner, H., Häkkinen, L., and Larjava, H. S.:** Expression of integrin alphavbeta6 and TGF-beta in scarless vs scar-forming wound healing, J. Histochem. Cytochem., **57**, 543–557 (2009).
4. **Irwin, C. R., Picardo, M., Ellis, I., Sloan, P., Grey, A., McGurk, M., and Schor, S. L.:** Inter- and intra-site heterogeneity in the expression of fetal-like phenotypic characteristics by gingival fibroblasts: potential significance for wound healing, J. Cell Sci., **107**, 1333–1346 (1994).
5. **Lorimier, S., Hornebeck, W., Godeau, G., Pellat, B., Gillery, P., Maquart, E. X., and Laurent-Maquin, D.:** Morphometric studies of collagen and fibrin lattices contracted by human gingival fibroblasts; comparison with dermal fibroblasts, J. Dent. Res., **77**, 1717–1729 (1998).
6. **Chang, H. Y., Chi, J.-T., Dudoit, S., Bondre, C., van de Rijn, M., Botstein, D., and Brown, P. O.:** Diversity, topographic differentiation, and positional memory in human fibroblasts, Proc. Natl. Acad. Sci. USA, **99**, 12877–12882 (2002).
7. **Yasuda, M., Miyachi, Y., Ishikawa, O., and Takahash, K.:** Spatial expressions of fibronectin and integrins by human and rodent dermal fibroblasts, Br. J. Dermatol., **155**, 522–531 (2006).
8. **Freshney, R. I.:** Culture of Animal Cells—A manual of basic technique—fifth edition, John Wiley & Sons, Inc., Hoboken (2005).
9. **O'Dell, S. D. and Day, I. N.:** Insulin-like growth factor II (IGF-II), Int. J. Biochem. Cell Biol., **30**, 767–771 (1998).
10. **Miller, A. G., Aplin, J. D., and Westwood, M.:** Adenovirally mediated expression of insulin-like growth factors enhances the function of first trimester placental fibroblasts, J. Clin. Endocrinol. Metab., **90**, 379–385 (2005).
11. **Nagase, H. and Woessner, J. F.:** Matrix metalloproteinases, J. Biol. Chem., **274**, 21491–21494 (1999).
12. **Skaleric, U., Manthey, C. M., Mergenhagen, S. E., Gaspirc, B., and Wahl, S. M.:** Superoxide release and superoxide dismutase expression by human gingival fibroblasts, Eur. J. Oral Sci., **108**, 130–135 (2000).
13. **Ebisawa, K., Kato, R., Okada, M., Ymada, Y., and Ueda, M.:** Regenerative medicine for anti-aging, Nippon Rinsho, **67**, 1402–1406 (2009).

Bone 49 (2011) 693–700

Contents lists available at ScienceDirect

Bone

journal homepage: www.elsevier.com/locate/bone

Stromal cell-derived factor-1 enhances distraction osteogenesis-mediated skeletal tissue regeneration through the recruitment of endothelial precursors

Masahito Fujio [a,1], Akihito Yamamoto [a,*,1], Yuji Ando [a], Ryutaro Shohara [a], Kazuhiko Kinoshita [a], Tadashi Kaneko [b], Hideharu Hibi [a], Minoru Ueda [a]

[a] Department of Oral and Maxillofacial Surgery, Nagoya University Graduate School of Medicine, 65 Tsurumai-cho, Showa-ku, Nagoya 466-8550, Japan
[b] Research and Development Dept. Biomaterial Group, GC Corporation, Tokyo, Japan

ARTICLE INFO

Article history:
Received 10 February 2011
Revised 16 June 2011
Accepted 18 June 2011
Available online 29 June 2011

Edited by: Thomas Einhorn

Keywords:
Distraction osteogenesis
Stromal cell-derived factor-1
Endothelial progenitor cells
Regeneration
Bone
Angiogenesis

ABSTRACT

Distraction osteogenesis (DO) is a unique therapy that induces skeletal tissue regeneration without stem/progenitor cell transplantation. Although the self-regeneration property of DO provides many clinical benefits, the long treatment period required is a major drawback. A high-speed DO mouse model (H-DO), in which the distraction was done two times faster than in control DO (C-DO) mice, failed to generate new bone callus in the DO gap. We found that this was caused by the unsuccessful recruitment of bone marrow endothelial cells (BM-ECs)/endothelial progenitor cells (EPCs) into the gap. We then tested the ability of a local application of stromal cell-derived factor-1 (SDF-1), a major chemo-attractant for BM-ECs/EPCs, to accelerate the bone regeneration in H-DO. Our data showed that, in H-DO, SDF-1 induced callus formation in the gap through the recruitment of BM-ECs/EPCs, the maturation of neo-blood vessels, and increased blood flow. These results indicate that the active recruitment of endogenous BM-ECs/EPCs may provide a substantial clinical benefit for shortening the treatment period of DO.

Introduction

Distraction osteogenesis (DO) is used in orthopedic and craniofacial surgery to reconstruct skeletal deformities and lengthen the skeleton [1–5]. DO induces substantial tissue-regeneration/generation activities without the need for stem cell transplantation. The DO procedure involves three sequential phases: latency, active distraction, and consolidation. The latency phase consists of osteotomy followed by fixation of the two resulting bone fragments using an external or internal fixator. During active distraction, fixator-driven mechanical forces gradually separate the two bone fragments, generating a distraction gap, in which neo-callus formation occurs through the direct differentiation of mesenchymal stem cells (MSCs) into osteoblast lineages; this is known as an intramembranous ossification process [5–7]. In the consolidation phase, remodeling of the newly generated callus promotes the maturation of the neo-bone tissues. The DO also promotes the generation and/or remodeling of the surrounding soft tissues, including nerve, muscle, blood-vessel, and skin tissues [8]. Although the DO operation provides many clinical benefits for skeletal tissue regeneration, patients undergoing this procedure must endure a long treatment period, an average of 12 months, with a large external fixator, which can increase the risk of severe osteomyelitis by providing a route of entry for pathogens. Therefore, improving the DO technique by decreasing the treatment period would be extremely valuable.

As with physiological responses to tissue injury and repair, neovessel formation is one of the earliest events in organogenesis, and it plays essential roles in tissue regeneration by enabling the delivery of oxygen, nutrients, soluble factors, and cells of various types to the site of regeneration. The vessel-formation process consists of two sequential phases: vasculogenesis and angiogenesis [9]. Vasculogenesis involves the recruitment of bone marrow endothelial cells (BM-ECs)/endothelial progenitor cells (EPCs), their differentiation into mature endothelial cells (ECs), and the formation of primitive tubular vessel structures. Angiogenesis involves the sprouting and remodeling of the primitive vessels, and the subsequent stabilization of the sprouts by mural cells (pericytes in medium-sized vessels and smooth muscle cells in larger ones). The interaction between BM-ECs/EPCs and mural cells stabilizes micro-vessels and prevents vessel leakage. These multiple processes cooperatively promote blood-vessel formation; however, the roles of each process in DO-mediated skeletal tissue regeneration are still largely unknown.

Bone marrow-derived EPCs, which are considered a key player in blood vessel regeneration, have been isolated from the peripheral blood mononuclear cells of adult species [10,11]. These cells are recruited to ischemic tissues to adjust hypoxic conditions. The hypoxia-inducible

* Corresponding author. Fax: +81 52 744 2352.
E-mail address: akihito@med.nagoya-u.ac.jp (A. Yamamoto).
[1] These authors contributed equally to this work.

8756-3282/$ – see front matter © 2011 Elsevier Inc. All rights reserved.
doi:10.1016/j.bone.2011.06.024

factor (HIF-1) pathway senses changes in local oxygen availability and responds to them via the transcriptional activation of two pro-angiogenic factors, vascular endothelial growth factor (VEGF)-A and SDF-1 [12–14]. In DO, both HIF-1α and VEGF signaling are activated by the traction-induced hypoxia, and required for successful DO-mediated callus formation [7,15,16]. The forced activation of HIF-1α increases vessel formation and promotes bone regeneration [16]. SDF-1, which belongs to the CXC subfamily of chemokines, has a major role in both vasculogenesis and angiogenesis [17]. SDF-1 binds to the G-protein-coupled seven-transmembrane receptors CXCR4 and CXCR7; this recruits and retains receptors expressed on bone marrow-derived EPCs into the neo-angiogenic niches in ischemic tissues. SDF-1 is also required for the branching morphogenesis of ECs/EPCs during angiogenesis [18,19]. Thus, SDF-1 has broad functions in the vessel formation. However, its clinical benefits in DO systems or in treating bone fractures have not been reported.

In this report we show that locally administered SDF-1 in a high-speed DO mouse model promotes the recruitment of BM-ECs/EPCs and neo-callus formation in the DO gap. These experimental findings suggest that regulating the trafficking of endogenous stem/progenitor cells may provide a powerful therapeutic strategy for improving skeletal regeneration without stem cell transplantation.

Materials and methods

Mouse DO model

All animal experiments were performed in accordance with the Guidelines for Animal Experimentation of the Nagoya University School of Medicine. Eighty-three 8–10-week-old female ICR mice (Chubu Kagaku Shizai Corporation), were used. The mouse DO model was generated and modified as described previously [20,21].

The fixator consisted of two incomplete acrylic resin rings (outer diameter 20 mm, inner diameter 10 mm, thickness 5 mm) and an expansion screw (600-301-30; Ortho Dentaurum). The total weight of the device, including the needles inserted into the tibia, was 2.7 g.

The animals were anesthetized with an intraperitoneal injection of pentobarbital at 40 mg/kg body weight. The right limb was shaved and prepared with iodine solution. An anterior longitudinal incision was made on the right leg, and the underlying muscles were bluntly separated with care not to remove all of the periosteum. Fibulotomy was performed with a pair of scissors. The tibia was fixed to the device with one pair of 25-gauge needles proximally, one pair of 27-gauge needles distally, and acrylic resin. After complete polymerization (approximately 5 min), an osteotomy was performed at the middle of the diaphysis. This was done using very small cutting forceps. The wound was closed with a 4-0 nylon suture.

Control DO protocol (C-DO)

After a latency period of 5 days, distraction was started at a rate of 0.2 mm/12 h. The lengthening was continued for 8 days, to increase the length by 3.2 mm. The mice were gently killed 5, 9, and 13 days after surgery.

Mouse high-speed DO model (H-DO) and SDF-1 treatment

To determine the effect of a local application of recombinant human SDF-1α (350-NS; R&D Systems), we generated a mouse H-DO model in which the rate of distraction was 0.4 mm/12 h. The lengthening was continued for 4 days. In the SDF-1-treated group, a collagen gel matrix (Cellmatrix Type I-A; Nitta Gelatin) containing 200 ng of SDF-1 protein was injected transcutaneously using a 27-gauge needle into the center of the distraction zone. The injections were performed every other day from day 4.

Histology

Tibial segments from DO and unoperated mice were harvested after the mouse was perfused with 4% paraformaldehyde solution. The samples were embedded in SCEM gel (8091140; Leica) and frozen in cooled isopentane. Non-decalcified tibial bone sections were generated using Kawamoto's film method (8091098; Leica) [22]. Cryostat sections (5-μm thick) were used for Hematoxylin–Eosin staining and Alcian Blue-Fast red staining.

Immunohistochemistry

The 5-μm-thick sections were fixed in 99.5% ethanol for 10 min at room temperature, washed, blocked with 5% bovine serum albumin/phosphate buffered saline for 30 min, and then stained with the primary antibodies in blocking buffer for 1 h. The sections were then stained with the secondary antibodies for 30 min, mounted with SCMM R3 (Leica), and fluorescence microscopy was performed with a BZ9000 (Keyence). The following antibodies were used for immunostaining: rat monoclonal antibody (mAb) against CD31 (390: eBioscience) and Sca-1 (D7: BD pharmingen), and purified rabbit polyclonal antibodies (Abs) against CXCR4 (abcam) CXCR7 (abcam), SDF-1 (eBioscience) and α-SMA (Millipore), and purified goat Ab against Sca-1 (R&D). Secondary antibodies were conjugated with either Alexa Fluor 488, 555 or 647 (Invitrogen). Cell nuclei were labeled with diamidinophenylidole (Invitrogen).

Laser speckle blood flow imaging

C-DO and SDF-1-treated and untreated H-DO mice ($n=3$, each group) were examined on day 13. After being anesthetized, the animals were placed in the supine position and the fixator was carefully removed. Changes in the surface blood flow in the DO gap were monitored by a laser speckle blood flow imaging system (OMEGAZONE OZ-1; OMEGAWAVE). Color-coded blood flow images were obtained in high-resolution mode (638 pixels 480 pixels; 1 image/s).

Quantitative real-time reverse transcription-polymerase chain reaction

Mid-diaphyseal sections of the tibiae, including regenerated tissue in the distraction gap, and 3 mm of bone segments proximal and distal to it were excised with intact periosteum and stored in liquid nitrogen until required for analysis. Total RNA was then extracted using TRIzol (Invitrogen), and first-strand cDNA synthesis was carried out with Superscript III RTase (Invitrogen). Quantitative real time transcription polymerase chain reaction (PCR) was performed in Stepone Plus (Applied Biosystems) with THUNDERBIRD qPCR Mix (TOYOBO) according to standard protocols. Contamination of genome DNA in the PCR reaction was checked by both melting curve and gel analysis of no-RT-controls. Standard curves were generated for each gene and the amplification was 90%–100% efficient. Relative quantification of gene expression was determined by comparison of threshold values. All results were normalized to glyceraldehyde-3-phosphate dehydrogenase (*gapdh*). Primer sets are listed in Table 1. Results of these studies were derived from the average of three replicate experiments. All graphic data for mRNA expression are presented as days after surgery and with numeric values presented as the relative fold expression to the reference day 0.

Quantification and statistical analysis

To quantify the cells expressing a given marker or marker combination, we used Image J software and fluorescence microscopy (BZ9000). Statistical analysis was performed using the SPSS statistical package. Comparisons were made using the Mann–Whitney test. Results were expressed as the mean ± standard deviation (SD: $P<0.05$ was considered statistically significant).

Table 1
Primers utilized in quantitative RT-PCR.

Gene	Forward sequence (5′-3′)	Reverse sequence (5′-3′)
gapdh	AACTTTGGCATTGTGGAAGG	GGATGCAGGGATGATGTTCT
pdgfr-a	GGGGAGAGTGAAGTGAGCTG	CTCCCGTTATTGTGCAAGGT
pdgfr-b	CCGGAACAAACACACCTTCT	GAGCACTGGTGAGTCGTTGA
vegfr-1	GGATGCAGGGGACTATACGA	CTGCTGGGATCCAGGATAAA
vegfr-2	ATCTTTGGTGGAAGCCACAG	GGAATCCATAGGCGAGATCA
sdf-1	GCTCTGCATCAGTGACGGTA	AGATGCTTGACGTTGGCTCT
cxcr4	TCCTGCCCACCATCTACTTC	TTTCAGCCAGCAGTTTCCTT
cxcr7	CCAGGAGAAGCACAGTAGCC	CTGACACTCTGGAGGCATCA

Abbreviations: *gapdh*, glyceraldehyde-3-phosphate dehydrogenase; *pdgfr-a*, platelet-derived growth factor receptor alpha; *pdgfr-b*, platelet-derived growth factor receptor beta; *vegfr-1*, vascular endothelial growth factor receptor 1; *vegfr-2*, vascular endothelial growth factor receptor 2; *sdf-1*, stromal cell-derived factor-1; *cxcr4*, cxc chemokine receptor 4; *cxcr7*, cxc chemokine receptor 7.

Results

New bone callus formation and integration of BM-ECs/EPCs in the gap are suppressed in the H-DO model

We generated a C-DO model as described [20,21]. After applying a custom-made bilateral monofixator to the right tibia of 8-week-old mice (Figs. 1A and B), an osteotomy was carried out using a cutting forceps, with minimum damage to the muscle, periosteal, and dermal tissue. After a subsequent 5-day latency period, the osteotomized fragments were distracted at 0.2 mm per 12 h for 8 days (C-DO; Fig. 1C). This operation resulted in the generation of new bone callus within the gap at the end of the consolidation period (Fig. 1D). Alcian Blue staining revealed a little chondrogenic activity in the periosteal but not in the endosteal region of the gap (Fig. 1E), indicating that our DO model induced most of the new bone callus formation through intramembranous ossification, as described previously [23]. It is well

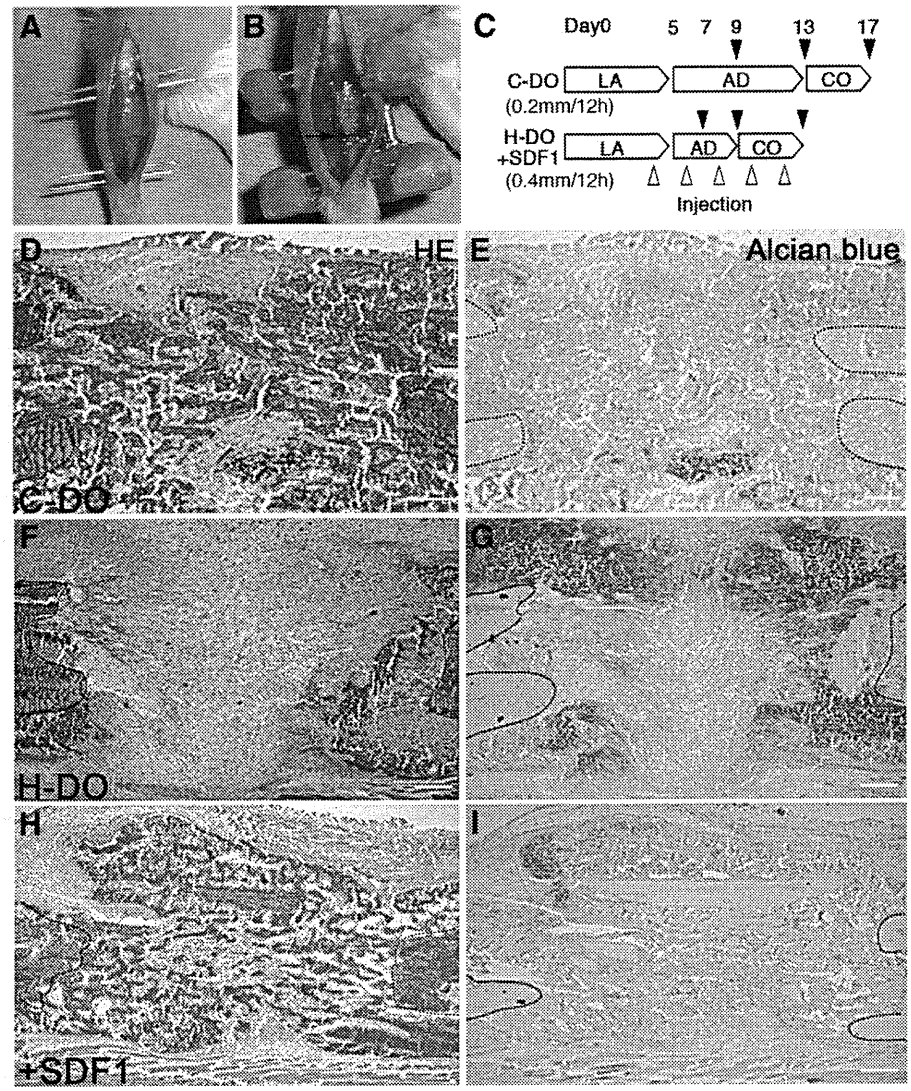

Fig. 1. Traction speed affects new bone callus formation in mouse DO models.(A, B) Surgical procedure for the mouse DO model. An anterior longitudinal incision was made on the right leg of the animal. Needles were inserted through the skin into the proximal and distal metaphysis of the tibia (A). Subsequently, sets of needles were fixed to the custom-made fixator with acrylic resin (B). After polymerization of the resin, osteotomy was carried out at the middle of the diaphysis (arrow).(C) Distraction protocols and experimental design. After a 5-day latency period, distraction was started at a rate of 0.2 mm/12 h (C-DO) or 0.4 mm/12 h (H-DO). The lengthening was continued for 8 days in the C-DO and 4 days in the H-DO model, resulting in a length increase of 3.2 mm. Black arrowheads indicate the time points of sacrifice. White arrowheads indicate the time points for injecting 200 ng SDF-1 protein (+SDF-1). LA, latency period; AD, active distraction period; CO, consolidation period.(D–I) Representative micrographs of sections displaying the DO gap stained with Hematoxylin–Eosin (HE) (D, F and H) and Alcian Blue–Fast red (E, G and I) ($n=8$). The left and right of each figure correspond to the end of the distal and proximal bone fragment, respectively. Neo-callus formation was evident within the C-DO gap at the end of the consolidation period (D). A little cartilage was observed in the periosteal but not in the endosteal region (E). The H-DO gap was filled with fibrotic tissues and periosteum-derived cartilages (F, G). The local administration SDF-1 rescued the callus formation in the H-DO gap (H, I). Bar = 300 μm (D–I).

known that the distraction rate determines the feasibility of the DO-mediated tissue-regeneration. High- and low-speed tractions lead to premature and impaired ossification in the gap, respectively [3,5,8]. We generated an H-DO model in which the bone fragments were distracted at 0.4 mm per 12 h, twice as fast as in the C-DO model (Fig. 1C). The H-DO model failed to generate callus in the gap, which was filled with periosteal-derived chondrogenic or fibrotic tissues (Figs. 1F and G).

Since chondrogenic development, instead of bone formation, in the DO-gap is closely associated with impaired neo-vasculature development, we assumed that the H-DO model would have defects in vasculogenesis or angiogenesis during the early distraction phase (see Discussion for details). To examine the integration of BM-ECs or EPCs in the early gap (day 7; Fig. 1C), we performed co-immunohistostaining with antibodies against CD31 (a marker for endothelial cells) and Sca-1 antigen (a marker for bone marrow stem and progenitor cells). The number of $CD31^+Sca\text{-}1^+$ BM-ECs/EPCs in the C-DO gap was 10-times higher than in intact bone marrow, whereas in the H-DO their number was significantly decreased compared with the C-DO gap ($P<0.01$), showing that the accumulation of endothelial precursors was severely impaired in the H-DO model (Figs. 2A, B, D and E).

Expression of SDF-1/CXCR4, 7 and angiogenic receptors in the DO gap

Real-time PCR analysis of the C-DO showed that the expressions of angiogenic receptors *vegfr-1* and *-2*, as well as of platelet-derived growth factor receptor *(pdgfr)-α* and *-β*, gradually increased during distraction (Fig. 3A). The levels of *sdf-1*, *cxcr4*, and *cxcr7* increased in a similar manner to those of the angiogenic receptors (Fig. 3B). Next, we immunohistologically examined the effect of distraction on the protein expression of SDF-1/CXCR4, 7 in the gap. CXCR4 (Figs. 3D–F) and CXCR7 (data not shown) were expressed on $44.5\pm12.5\%$ and $63.0\pm15.0\%$ of the $Sca\text{-}1^+$ stem/progenitor cells in the gap of the active distraction period, respectively (Fig. 3C). In intact bone marrow, SDF-1 is known to be expressed by BM-ECs, osteoblasts, and reticulocytes [12,24,25]. In our DO model, SDF-1 was mostly expressed in fibroblast-like cells surrounding the distal bone fragment (Fig. 3G). As few as $9.7\pm2.0\%$ of the BM-ECs (CD31 positive) expressed SDF-1 (Figs. 3I–K).

In the H-DO, the level of *sdf-1* mRNA expression was similar to that of C-DO (data not shown). Cells expressing SDF-1 accumulated locally in the bone marrow cavity adjacent to the H-DO gap, but were rarely observed within it (Fig. 3H). These results suggest that the reduction of SDF-1 expression in the H-DO gap may be involved in the impaired recruitment of BM-ECs/EPCs.

Recovery of neo-callus formation in the H-DO gap by the angiogenic activities of SDF-1

We tested whether the local administration of SDF-1, a chemo-attractant for BM-ECs/EPCs, would rescue the disrupted callus formation and integration of BM-ECs/EPCs in the H-DO gap. A collagen gel matrix containing 200 ng of SDF-1 protein was injected into the H-DO gap every other day (Fig. 1C). We found that the high levels of SDF-1 rescued the callus formation and increased the number of BM-ECs/EPCs in the H-DO gap (Figs. 1H, I and 2C). Although about 80% of the $CD31^+$ cells co-expressed Sca-1 in the C-DO gap, in the H-DO gap treated with SDF-1, 50% of the $CD31^+$ cells were negative for Sca-1, suggesting that some of the BM-ECs/EPCs recruited by SDF-1 had already differentiated into mature endothelial cells (Fig. 2E).

We next examined whether SDF-1 promotes the formation of mature vessels composed of two types of cells, $CD31^+$ endothelial cells and αSMA^+ pericytes. Endothelial cells line the vessel lumen as a continuous layer, while pericytes, which are of mesenchymal origin, constitute the outer layer of micro-vessels. The pericytes play important roles in vessel maturation, remodeling, and stabilization

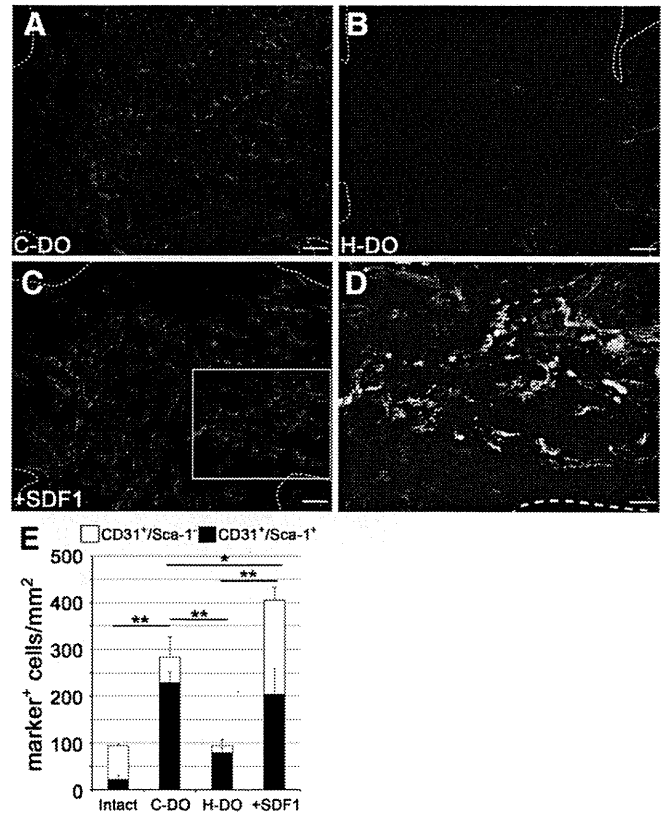

Fig. 2. Contribution of BM-ECs/EPCs to DO healing.Mice were sacrificed at the middle of the active distraction period in each group: day 9 and day 7, respectively, for the C-DO and H-DO group. (A, B, and C) The recruitment of BM-ECs/EPCs was evaluated by immunofluorescence staining for CD31 (red) ($n=6$). CD31-positive BM-ECs/EPCs accumulated in the C-DO (A), but not in the H-DO gap (B). Local administration of SDF-1 rescued the recruitment of BM-ECs/EPCs to the H-DO gap (C) ($n=8$). (D) Boxed area in (C) is shown in higher-magnification micrographs, in which the CD31 signals are seen together with Sca-1 (green). Note that SDF-1 treatment increased the number of $CD31^+Sca\text{-}1^-$ cells in the gap. (E) CD31-single-positive and $CD31^+Sca\text{-}1^+$ cells were counted by Image J software. The number of $CD31^+Sca\text{-}1^+$ BM-ECs/EPCs in the C-DO gap was significantly higher than that in intact bone marrow, whereas that in the H-DO gap was significantly lower. SDF-1 treatment rescued the number of BM-ECs/EPCs in the H-DO gap. The dotted line represents native bone. Data represent the mean ± SD. $^{**}P<0.01$ and $^{*}P<0.05$. Intact: intact bone marrow. Bar = 100 μm (A, B, C) and 50 μm (D).

[26–28]. At the end of consolidation, we found that $CD31^+$ cells appeared in the H-DO gap as cellular aggregates that failed to form a mature vessel network (Figs. 4A and B), whereas in the SDF-1-treated gap, there were many tubular micro-vessel structures. Importantly, these neo-vessels were composed of an internal endothelial cell layer and an outer pericyte layer (Figs. 4C–E). These results demonstrate that the local administration of SDF-1 protein in the H-DO model activates the recruitment of both endothelial precursors and pericytes to the site of tissue regeneration and promotes the maturation of neo-blood vessels.

SDF-1 rescues the ischemic condition of the H-DO model

We examined whether the local administration of SDF-1 increases blood flow, using a laser speckle perfusion imager. At the end of active distraction period, severe reductions in blood flow were seen in the H-DO gap compared with the C-DO gap (Figs. 5A–D). SDF-1 treatment dramatically increased the blood flow in the gap in the H-DO group (Figs. 5E–G) ($P<0.01$). Taken together, these results demonstrate that SDF-1 rescues the extreme ischemic condition in the H-DO gap, thereby restoring new bone callus formation.

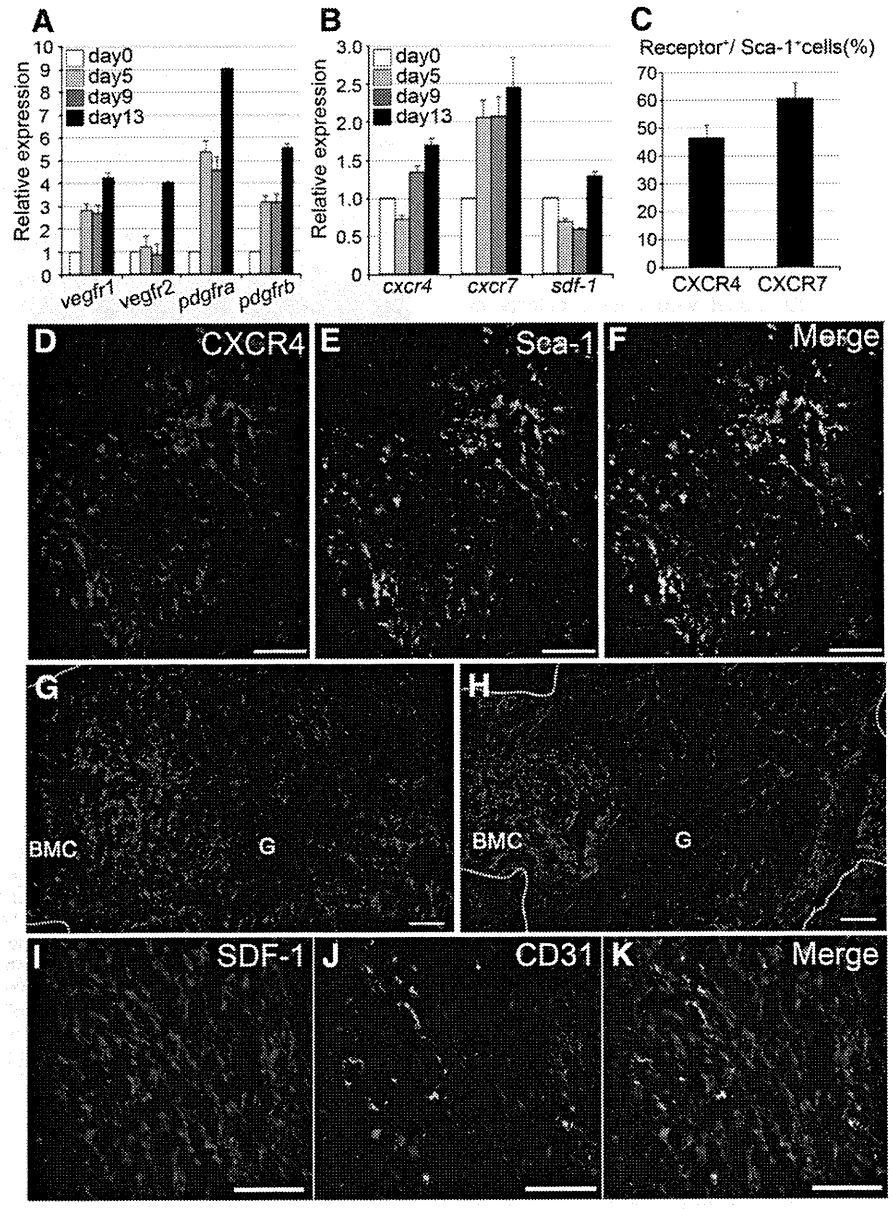

Fig. 3. Expression of the SDF-1/CXCR4, 7 axis in the gap.(A, B) The expressions of angiogenic receptors and of *sdf-1*, *cxcr4*, and *cxcr7* were analyzed by real-time PCR. C-DO treatment increased the expression of angiogenic receptors (A) and of *sdf-1*, *cxcr4*, and *cxcr7* (B). (C–F) Cells recruited into the C-DO gap were characterized by immunohistochemical staining with an anti-CXCR4 or CXCR7 Ab together with an anti-Sca-1 mAb. (C) The total Sca-1^+ cells and the number of Sca-1^+ cells expressing CXCR4 or CXCR7 were counted by Image J software. (D–F) Representative images show the accumulation of cells expressing both CXCR4 (red) and Sca-1 (green) in the C-DO gap. (G, H) SDF-1 expression in the C-DO (G) and H-DO gap (H) during the distraction phase ($n = 6$). Fibroblast-like cells surrounding the distal bone fragment expressed SDF-1. These SDF-1^+ cells accumulated in the bone marrow cavity adjacent to the H-DO gap, but were rarely observed in it. BMC, bone marrow cavity; G, gap region. Co-immunohistochemical staining with anti-SDF-1 Ab and anti-CD31 mAb is shown (I–K). Bar = 100 μm.

Discussion

In this study we report the clinical benefits of the local administration of SDF-1 in the acceleration of new bone callus formation in the DO gap using mouse model. In the H-DO gap, delayed integration and aggregate formation of endogenous BM-ECs/EPCs resulted in subsequent severe ischemia that prevents DO-mediated tissue regeneration. This regeneration failure was coincident with a severe decrease in SDF-1 expression in the gap. The local administration of SDF-1 dramatically restored or enhanced the integration of BM-ECs/EPCs, maturation of blood vessels, blood flow, and callus formation. Our findings present a novel application of SDF-1 protein for enhancing the clinical efficiency of DO for correcting limb length inequalities, severe deformities, and bone defects.

It has been well established that an active blood vessel network is an essential prerequisite for osteogenesis as well as general tissue repair [9,29,30]. The vasculature transports oxygen, nutrients, soluble growth factors, and various types of cells, which collectively play pivotal roles in tissue regeneration. In DO, it has been shown that the rate of distraction controls blood vessel formation in the gap [3,5,8]. In particular, DO performed with a high distraction rate results in a severe deficiency in vessel formation, as we observed in our H-DO model [5]. Our immunohistochemical analysis demonstrates that the H-DO procedure inhibits pro-angiogenic events, BM-ECs/EPCs integration and vessel maturation in the gap. Interestingly, we found massive chondrogenesis in the H-DO gap, indicating that at least the trafficking of mesenchymal progenitors toward the H-DO gap was preserved to some extent. These vascular and skeletal properties are

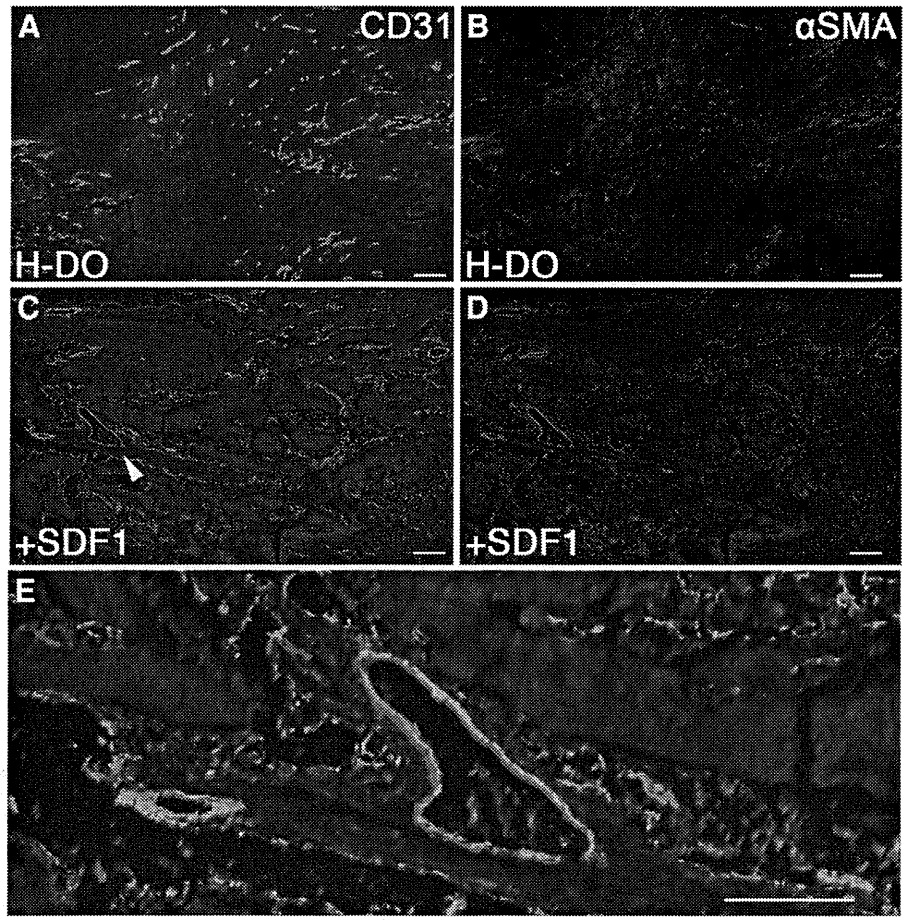

Fig. 4. SDF-1 promotes blood vessel maturation.Immunohistochemical staining for CD31 (green) and αSMA (red) was performed at the end of the consolidation period. ($n=6$) (A, B) H-DO samples showed cellular aggregates of BM-ECs/EPCs, which failed to form a mature vessel network. (C, D, E) The local administration of SDF-1 promoted the formation of mature blood vessels (white arrowhead in 3C) that consisted of CD31-positive endothelial cells and αSMA-positive pericytes. Bar = 300 μm (A–D) and 100 μm (E).

reminiscent of the knockdown phenotype of the pro-angiogenic factor, VEGF, in which similar chondrogenesis occurs in the gap instead of callus formation [7]. Thus, these results show that the primary cause of tissue regeneration failure in H-DO is a defect in the early integration and maturation of endothelial progenitors in the gap.

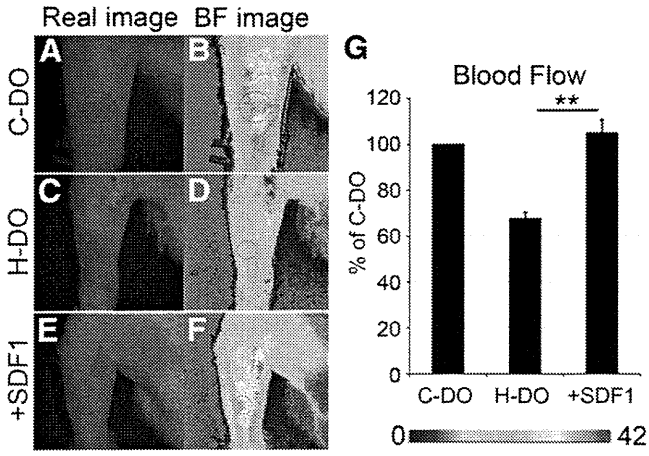

Fig. 5. Locally administered SDF-1 rescues the ischemic condition of H-DO mice. Color-coded representative images and quantification of the blood flow are shown ($n=3$). (A–D) At the end of the active distraction period, the H-DO gap showed severely reduced blood flow compared with the C-DO gap. (E, F) The local administration of SDF-1 caused recovery of the H-DO mice from the ischemic condition. (G) The blood flow index was expressed as a percentage, in which the value in C-DO was considered 100%. Data represent the mean ± SD. $^{**}P<0.01$.

Recent studies have shown that locally transplanted ex-vivo-expanded EPCs or BM-derived mononuclear cells accelerate neo-vessel formation and can elicit profound clinical benefits in the treatment of a variety of ischemic diseases [31]. In bone regeneration and repair, intravenously infused EPCs are recruited to the site of fracture and DO [32,33], suggesting that they also play important roles in new bone formation. These previous studies highlight the transplantation of EPCs as a promising treatment in regenerative medicine; however, for clinical use they must be expanded by a reliable cell culture system that produces sufficient cell numbers for clinical benefits, while also meeting safety requirements [34]. These severe restrictions may impede the progress of regenerative therapy based on therapeutic vasculogenesis. Our data demonstrate that, instead of the local transplantation or systemic administration of EPCs, the SDF-1-mediated recruitment of endogenous BM-ECs/EPCs may provide a significant therapeutic benefit, leading to the development of a safe and practical skeletal regeneration therapy.

To restore blood flow, the recruitment of BM-ECs/EPCs alone is not sufficient; the initial endothelial tubes must sprout and be covered with mural cells. The formation of mature vessels is a complex process, requiring the finely tuned integration of multiple signaling pathways [9,26–28]. Our data demonstrate that the local administration of SDF-1 elicits multi-angiogenic activities, which restore blood flow in the H-DO gap. In addition to the recruitment of BM-ECs/EPCs, SDF-1 promoted the differentiation of BM-ECs/EPCs, as evidenced by an increase in the number of $CD31^{+}Sca\text{-}1^{-}$ cells (Fig. 2), and the maturation of neo-

vessels by the recruitment of α-SMA$^+$ pericytes (Fig. 4). These two types of SDF-1-mediated angiogenic activities have been reported in other ischemic disease models [35,36]. Furthermore, it has been shown that SDF-1 controls vessel patterning by regulating tip-cell morphology and branching [18,19]. VEGF is another major pro-angiogenic factor that plays an essential role in the DO-mediated tissue regeneration [7]. VEGF protein can activate only some aspects of vessel formation, the proliferation/differentiation of endothelial precursors, and tip-cell formation [37]. The local administration of VEGF alone fails to activate bone regeneration in a DO system [38]. Our data imply that, because tissue injury and repair are associated with the disruption of the permissive microenvironment necessary for vessel formation, the activation of the entire process, including both vasculogenesis and angiogenesis, is required to establish the active blood vessel network needed to support bone regeneration.

The regulated movement of stem cells is critical for tissue regeneration and repair. The SDF-1/CXCR4, 7 systems have been implicated in the mobilization of adult tissue-committed stem cells and progenitors, including hematopoietic stem cells, MSCs, and EPCs [39–43]. In the C-DO animals, we found that the expression of SDF-1 and CXCR4, 7 increased during the distraction period in a manner similar to that of angiogenic receptors (Fig. 3). Most of the Sca-1-positive BM cells expressed the CXCR4 or 7 receptor. Notably, SDF-1 expression was observed on many fibroblast-like cells in the C-DO gap, while it was dramatically lower in the H-DO gap. These results suggest that SDF-1 may function as a chemo-attractant for multiple stem-cell lineages in the DO. However, we were unable to obtain a convincing result demonstrating SDF-1's involvement in the mobilization of MSCs. This is because there is no simple, appropriate marker for MSCs [44] and because MSCs/mesenchymal progenitors trafficking was maintained in the H-DO gap, as evidenced by the formation of cartilage (Fig. 1). Recent studies have revealed possible candidates for MSC markers [45,46]. In the future, such markers may allow us to clarify the factor involved in recruiting the MSCs in DO-mediated tissue regeneration.

DO and fracture healing generate bone tissue by intramembranous and endochondral ossification, respectively. However, in our H-DO model, endochondral ossification occurred instead of intramembranous ossification. The molecular mechanisms and regulatory factors determining the mode of ossification are still unclear. In our preliminary in vitro analysis, the direct application of SDF-1 accelerated the migration of cultured MSCs, but it did not promote osteogenic differentiation (unpublished observation). This result suggests that the local application of SDF-1 affects the differentiation of the recruited MSCs by indirect mechanisms. Our data suggest that the BM-ECs/EPCs recruited by SDF-1 may determine the mode of the ossification in the gap. In agreement with this idea, previous studies have shown that an increased expression of multiple pro-angiogenic factors occurs in the DO-gap during the distraction period, but not at fracture sites during the immediate-early phase of healing [5,15]. Furthermore, the co-culture of MSCs and ECs in vitro promotes the osteogenic differentiation of MSCs [47], supporting the idea that ECs directly regulate this differentiation. In early endochondral ossification, mesenchymal cells begin to condense while there is little or no vessel innervation [48,49]. These previous reports together with our experimental data strongly suggest that the recruited BM-ECs/EPCs and/or differentiated ECs control the mode of ossification/osteogenic differentiation of MSCs at the site of tissue regeneration.

In summary, our study demonstrated that locally administered SDF-1 promotes the recruitment of endogenous BM-ECs/EPCs and neo callus formation in the DO gap. We propose that the regulation of endogenous stem/progenitor cell trafficking is a powerful therapeutic strategy in skeletal regeneration.

Acknowledgments

We are grateful to Professor Akira Yamaguchi (Tokyo Medical and Dental University) for their critical comments for the manuscript. We also thank Drs. Kiyoshi Sakai and Masayuki Ikeno, and Ms. Mami Naruse for their encouragement to complete this study. We thank the Division of Experimental Animals and Medical Research Engineering, Nagoya University Graduate School of Medicine, for the housing of mice and for microscope maintenance. This work was supported by Grants-in-Aid for Scientific Research on Priority Areas from the Ministry of Education, Culture, Sports, Science and Technology of Japan and COE for education and research of Micro-Nano Mechatronics Nagoya University Global COE Program.

References

[1] Ilizarov GA. Clinical-application of the tension-stress effect for limb lengthening. Clin Orthop Relat Res 1990:8–26.
[2] McCarthy JG, Stelnicki EJ, Mehrara BJ, Longaker MT. Distraction osteogenesis of the craniofacial skeleton. Plast Reconstr Surg 2001;107:1812–27.
[3] Samchukov ML, Makarov MR, Cherkashin AM, Birch JG. Distraction osteogenesis of the orthopedic skeleton: basic principles and clinical applications; 2008.
[4] Ai-Aql ZS, Alagl AS, Graves DT, Gerstenfeld LC, Einhorn TA. Molecular mechanisms controlling bone formation during fracture healing and distraction osteogenesis. J Dent Res 2008;87:107–18.
[5] Li G, Simpson AH, Kenwright J, Triffitt JT. Effect of lengthening rate on angiogenesis during distraction osteogenesis. J Orthop Res 1999;17:362–7.
[6] Lewinson D, Maor G, Rozen N, Rabinovich I, Stahl S, Rachmiel A. Expression of vascular antigens by bone cells during bone regeneration in a membranous bone distraction system. Histochem Cell Biol 2001;116:381–8.
[7] Jacobsen KA, Al-Aql ZS, Wan C, Fitch JL, Stapleton SN, Mason ZD, et al. Bone formation during distraction osteogenesis is dependent on both VEGFR1 and VEGFR2 signaling. J Bone Miner Res 2008;23:596–609.
[8] Ilizarov GA. The tension stress effect on the genesis and growth of tissues. 2. The influence of the rate and frequency of distraction. Clin Orthop Relat Res 1989: 263–85.
[9] Carmeliet P. Angiogenesis in health and disease. Nat Med 2003;9:653–60.
[10] Asahara T, Murohara T, Sullivan A, Silver M, van der Zee R, Li T, et al. Isolation of putative progenitor endothelial cells for angiogenesis. Science 1997;275:964–7.
[11] Murohara T, Ikeda H, Duan J, Shintani S, Sasaki K, Eguchi H, et al. Transplanted cord blood-derived endothelial precursor cells augment postnatal neovascularization. J Clin Invest 2000;105:1527–36.
[12] Ceradini DJ, Kulkarni AR, Callaghan MJ, Tepper OM, Bastidas N, Kleinman ME, et al. Progenitor cell trafficking is regulated by hypoxic gradients through HIF-1 induction of SDF-1. Nat Med 2004;10:858–64.
[13] Wang Y, Wan C, Deng L, Liu X, Cao X, Gilbert SR, et al. The hypoxia-inducible factor alpha pathway couples angiogenesis to osteogenesis during skeletal development. J Clin Invest 2007;117:1616–26.
[14] Riddle RC, Khatri R, Schipani E, Clemens TL. Role of hypoxia-inducible factor-1 alpha in angiogenic-osteogenic coupling. J Mol Med 2009;87:583–90.
[15] Carvalho RS, Einhorn TA, Lehmann W, Edgar C, Al-Yamani A, Apazidis A, et al. The role of angiogenesis in a murine tibial model of distraction osteogenesis. Bone 2004;34:849–61.
[16] Wan C, Gilbert SR, Wang Y, Cao X, Shen X, Ramaswamy G, et al. Activation of the hypoxia-inducible factor-1alpha pathway accelerates bone regeneration. Proc Natl Acad Sci U S A 2008;105:686–91.
[17] Petit I, Jin D, Rafii S. The SDF-1-CXCR4 signaling pathway: a molecular hub modulating neo-angiogenesis. Trends Immunol 2007;28:299–307.
[18] Salvucci O, Yao L, Villalba S, Sajewicz A, Pittaluga S, Tosato G. Regulation of endothelial cell branching morphogenesis by endogenous chemokine stromal-derived factor-1. Blood 2002;99:2703–11.
[19] Strasser GA, Kaminker JS, Tessier-Lavigne M. Microarray analysis of retinal endothelial tip cells identifies CXCR4 as a mediator of tip cell morphology and branching. Blood 2010;115:5102–10.
[20] Tay BK, Le AX, Gould SE, Helms JA. Histochemical and molecular analyses of distraction osteogenesis in a mouse model. J Orthop Res 1998;16:636–42.
[21] Isefuku S, Joyner CJ, Simpson AH. A murine model of distraction osteogenesis. Bone 2000;27:661–5.
[22] Kawamoto T. Use of a new adhesive film for the preparation of multi-purpose fresh-frozen sections from hard tissues, whole-animals, insects and plants. Arch Histol Cytol 2003;66:123–43.
[23] Pacicca DM, Patel N, Lee C, Salisbury K, Lehmann W, Carvalho R, et al. Expression of angiogenic factors during distraction osteogenesis. Bone 2003;33:889–98.
[24] Sugiyama T, Kohara H, Noda M, Nagasawa T. Maintenance of the hematopoietic stem cell pool by CXCL12-CXCR4 chemokine signaling in bone marrow stromal cell niches. Immunity 2006;25:977–88.
[25] Jung Y, Wang J, Schneider A, Sun YX, Koh-Paige AJ, Osman NI, et al. Regulation of SDF-1 (CXCL12) production by osteoblasts; a possible mechanism for stem cell homing. Bone 2006;38:497–508.
[26] Allt G, Lawrenson JG. Pericytes: cell biology and pathology. Cells Tissues Organs 2001;169:1–11.
[27] Gerhardt H, Betsholtz C. Endothelial-pericyte interactions in angiogenesis. Cell Tissue Res 2003;314:15–23.
[28] Armulik A, Abramsson A, Betsholtz C. Endothelial/pericyte interactions. Circ Res 2005;97:512–23.
[29] Carano RAD, Filvaroff EH. Angiogenesis and bone repair. Drug Discov Today 2003;8:980–9.

[30] Kanczler JM, Oreffo ROC. Osteogenesis and angiogenesis: the potential for engineering bone. Eur Cell Mater 2008;15:100–14.
[31] Rafii S, Lyden D. Therapeutic stem and progenitor cell transplantation for organ vascularization and regeneration. Nat Med 2003;9:702–12.
[32] Lee DY, Cho TJ, Kim JA, Lee HR, Yoo WJ, Chung CY, et al. Mobilization of endothelial progenitor cells in fracture healing and distraction osteogenesis. Bone 2008;42: 932–41.
[33] Matsumoto T, Mifune Y, Kawamoto A, Kuroda R, Shoji T, Iwasaki H, et al. Fracture induced mobilization and incorporation of bone marrow-derived endothelial progenitor cells for bone healing. J Cell Physiol 2008;215:234–42.
[34] Bongso A, Fong CY, Gauthaman K. Taking stem cells to the clinic: major challenges. J Cell Biochem 2008;105:1352–60.
[35] De Falco E, Porcelli D, Torella AR, Straino S, Iachininoto MG, Orlandi A, et al. SDF-1 involvement in endothelial phenotype and ischemia-induced recruitment of bone marrow progenitor cells. Blood 2004;104:3472–82.
[36] Song N, Huang Y, Shi H, Yuan S, Ding Y, Song X, et al. Overexpression of platelet-derived growth factor-BB increases tumor pericyte content via stromal-derived factor-1alpha/CXCR4 axis. Cancer Res 2009;69:6057–64.
[37] De Smet F, Segura I, De Bock K, Hohensinner PJ, Carmeliet P. Mechanisms of vessel branching: filopodia on endothelial tip cells lead the way. Arterioscler Thromb Vasc Biol 2009;29:639–49.
[38] Eckardt H, Bundgaard KG, Christensen KS, Lind M, Hansen ES, Hvid I. Effects of locally applied vascular endothelial growth factor (VEGF) and VEGF-inhibitor to the rabbit tibia during distraction osteogenesis. J Orthop Res 2003;21:335–40.
[39] Abbott JD, Huang Y, Liu D, Hickey R, Krause DS, Giordano FJ. Stromal cell-derived factor-1alpha plays a critical role in stem cell recruitment to the heart after myocardial infarction but is not sufficient to induce homing in the absence of injury. Circulation 2004;110:3300–5.
[40] Kucia M, Reca R, Miekus K, Wanzeck J, Wojakowski W, Janowska-Wieczorek A, et al. Trafficking of normal stem cells and metastasis of cancer stem cells involve similar mechanisms: pivotal role of the SDF-1-CXCR4 axis. Stem Cells 2005;23:879–94.
[41] Smart N, Riley PR. The stem cell movement. Circ Res 2008;102:1155–68.
[42] Bladergroen BA, Siebum B, Siebers-Vermeulen KG, Van Kuppevelt TH, Poot AA, Feijen J, et al. In vivo recruitment of hematopoietic cells using stromal cell-derived factor 1 alpha-loaded heparinized three-dimensional collagen scaffolds. Tissue Eng Part A 2009;15:1591–9.
[43] Kitaori T, Ito H, Schwarz EM, Tsutsumi R, Yoshitomi H, Oishi S, et al. Stromal cell-derived factor 1/CXCR4 signaling is critical for the recruitment of mesenchymal stem cells to the fracture site during skeletal repair in a mouse model. Arthritis Rheum 2009;60:813–23.
[44] Dominici M, Le Blanc K, Mueller I, Slaper-Cortenbach I, Marini F, Krause D, et al. Minimal criteria for defining multipotent mesenchymal stromal cells. The International Society for Cellular Therapy position statement. Cytotherapy 2006;8:315–7.
[45] Morikawa S, Mabuchi Y, Kubota Y, Nagai Y, Niibe K, Hiratsu E, et al. Prospective identification, isolation, and systemic transplantation of multipotent mesenchymal stem cells in murine bone marrow. J Exp Med 2009;206:2483–96.
[46] Mendez-Ferrer S, Michurina TV, Ferraro F, Mazloom AR, Macarthur BD, Lira SA, et al. Mesenchymal and haematopoietic stem cells form a unique bone marrow niche. Nature 2010;466:829–34.
[47] Kaigler D, Krebsbach PH, West ER, Horger K, Huang YC, Mooney DJ. Endothelial cell modulation of bone marrow stromal cell osteogenic potential. FASEB J 2005;19: 665–7.
[48] Magne D, Vinatier C, Julien M, Weiss P, Guicheux J. Mesenchymal stem cell therapy to rebuild cartilage. Trends Mol Med 2005;11:519–26.
[49] Karsenty G, Kronenberg HM, Settembre C. Genetic control of bone formation. Annu Rev Cell Dev Biol 2009;25:629–48.

Supraperiosteal Transport Distraction Osteogenesis for Reconstructing a Segmental Defect of the Mandible

Hideharu Hibi, DDS, PhD, and Minoru Ueda, DDS, PhD†*

Distraction osteogenesis using the maximal osteogenic potential of the periosteum is introduced and demonstrated in 2 clinical cases. This technique includes minimizing cuts to and reflection of the periosteum on a transport segment; repositioning and suturing the cut periosteum to cover an osteotomy line, which becomes the distraction gap; and fixing an internal distraction device supraperiosteally. The cases involve reconstruction of a segmental defect of the mandible due to a recurrent ameloblastoma. A 51 + 58-mm posterior body and ramus and a 41 + 33-mm anterior body are reconstructed through 2-step and bilateral distraction osteogenesis, respectively. These cases proved the feasibility of the concept of the supraperiosteal transport distraction osteogenesis.

J Oral Maxillofac Surg 69:742-746, 2011

Distraction osteogenesis (DO) is a useful technique for reconstructing bony defects without performing grafting procedures in the maxillofacial region. When this technique provides new bone formation in a distracted area, the primary blood supply must be considered. Adequate blood supply to transport segments via intramedullary and periosteal routes is crucial to produce sufficient bone formation in a distraction gap.[1,2] Although medullary continuity that may be maintained with corticotomy[1-3] cannot always be performed in this region, periosteal attachment and continuity can be controlled by a surgeon. We present a transport DO method for mandibular reconstruction using supraperiosteal application of internal distraction devices to minimize disturbances of the periosteal blood supply to transport segments.

Surgical Technique and Distraction

A mucosal or skin incision and subsequent supraperiosteal dissection are performed to provide an area for seating the distraction device. A minimal periosteal incision is made a few millimeters from a planned osteotomy line to create a transport segment, and the periosteum is then reflected beyond this line (Fig 1). After the osteotomy, the periosteum is repositioned and sutured. When a distraction device is fixed supraperiosteally, special care should be taken not to compress the underlying periosteum with the plates, and fixation screws should therefore not be fully tightened unless they contain a locking mechanism with the plates. The wound is closed in layers.

The transport segment should move within the limits of periosteal tension according to activation of the distraction device performed over several weeks until the transport completes to cross a segmental defect for reconstruction. Six or more months of healing is required before device removal.

Case Reports

CASE 1. TWO-STEP TRANSPORT DO FOR MANDIBULAR POSTERIOR BODY AND RAMUS

A 39-year-old woman had a recurrent ameloblastoma of the posterior mandible (Fig 2A) and underwent a mandibular segmental resection to remove it and a distraction device fixation for reconstruction through a submandibular approach. A periosteal cut and a vertical osteotomy were performed buccally 17 and 15 mm from the resected edge of the mandible, respectively. The 2-mm-long buccal periosteal flap of the transport segment was repositioned and sutured; a custom-made distraction device[4] was adjusted with an artificial condyle (Dynamic Bridging Plate Mandibular Reconstruction System; Stryker Leibinger, Freiburg, Germany) and seated (Fig 2B). The transport segment was supraperiosteally fixed with locking plates and screws (Universal Plating System; Stryker Leibinger; Fig 2C). After a 7-day latency period, the device was activated at a rate of 0.5 mm twice a day for 50 days until the transport segment had reached the mandibular angle, when the percutaneous

Received from the Department of Oral and Maxillofacial Surgery, Nagoya University Graduate School of Medicine, Nagoya, Japan.

*Associate Professor.

†Professor.

Address correspondence and reprint requests to Dr Hibi: Department of Oral and Maxillofacial Surgery, Nagoya University Graduate School of Medicine, 65 Tsurumai-cho, Showa-ku, Nagoya 466-8550, Japan; e-mail: hibihi@med.nagoya-u.ac.jp

0278-2391/11/6903-0018$36.00/0

doi:10.1016/j.joms.2010.07.059